Leman-Baikal Project

Annual report 2014

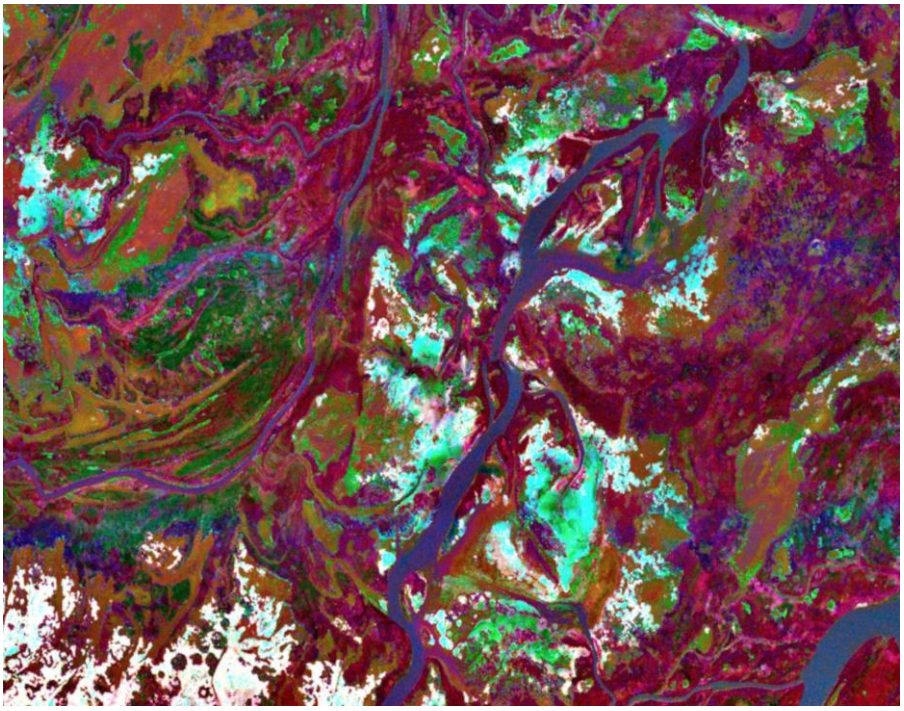

Hyperspectral image of the Selenga Delta (Lake Baikal)

Publisher: Ecole Polytechnique Fédérale de Lausanne, Limnology Center, CH-1015 Lausanne, 15 November 2014

Sponsored by:

Coordinated by: Limnology Centre and Consulat honoraire de la Fédération de Russie à Lausanne

1. Résumé

Le projet Léman-Baïkal est une collaboration internationale entre la Suisse et la Russie, visant à mesurer les propriétés des lacs à l'aide d'ultra-léger motorisés (ULM). Son but principal est de comparer la qualité des eaux et le bilan énergétique du Lac Léman en Suisse et du Lac Baïkal au Sud de la Sibérie dans la Fédération de Russie. La télédétection à partir d'un ULM permet de cartographier l'hétérogénéité spatiale des propriétés à haute résolution, qui est particulièrement important aux interfaces entre les terres et le lac.

Ce projet multidisciplinaire regroupe différents laboratoires de l'Ecole Polytechnique Fédérale de Lausanne et des équipes du « Baikal Institute for Nature Management » et « Lomonosov Moscow State University ». Quatre laboratoires de l'EPFL (TOPO, LASIG, APHYS, ECOL) se concentrent sur la télédétection pour créer des cartes de la chlorophylle a, la matière en suspension, le carbone organique dissous et la température à la surface des deux lacs. Trois laboratoires (WIRE, EFLUM, CRYOS) en collaboration avec l'Université de Princeton étudient les turbulences à l'interface entre l'air et l'eau sur le Lac Léman.

Après une phase de test en 2013, la plateforme de télédétection a encore été améliorée et a enregistré des images multispectrales et hyperspectrales au-dessus de la surface des lacs. En 2014, 17 vols ont eu lieu sur le Lac Léman pendant 3 campagnes en février/mars, avril/mai et septembre. Les vols se sont concentrés sur les embouchures des rivières de la Venoge et du Rhône, où le mélange d'eaux de différentes qualités crée d'intéressantes structures. Pour obtenir une vue plus globale, nous avons aussi couvert le lac entier.

Au Lac Baïkal, nous avons acquis des images multispectrales et hyperspectrale sur la totalité du Delta de la Selenga en août 2014. Le delta est composé d'une incroyable diversité de plantes, arbres, canaux et eaux stagnantes qui a pu être captée par nos images. Le succès de cette campagne a été assuré par la collaboration avec les étudiants russes impliqués dans ce projet.

Le traitement de cette énorme quantité de données va bientôt fournir les premières cartes de la qualité des eaux. Les équipes de télédétection et de calibration sur le terrain travaillent ensemble sur la dernière étape d'une longue chaîne de traitement. Cependant, des étapes itératives sont encore nécessaires pour assurer une bonne qualité des résultats. Pour interpréter les données du Delta de la Selenga, 4 étudiants russes viendront faire un stage à l'EPFL à partir de mi-Novembre. Nous espérons donc que les résultats évalueront bientôt l'hétérogénéité de la qualité des eaux des deux lacs à une résolution spatiale et temporelle encore jamais obtenues.

Concernant la couche limite de l'atmosphère, les turbulences ont été mesurées pendant les deux premières campagnes sur le Lac Léman. Cependant, l'ULM s'est révélé peu adapté aux mesures atmosphériques à cause des vibrations. De plus, les conditions météorologiques avec de fortes vitesses des vents, qui seraient les plus intéressantes, sont trop dangereuses en ULM.

En 2015, les équipes de télédétection planifie d'acquérir des données additionnelles sur le Lac Léman pendant une dernière campagne en avril/mai. Une autre campagne le long de toutes les côtes du Lac Baïkal est prévue en juillet et août 2015 en étroite collaboration avec nos collègues russes. Cette année, l'accent sera également mis sur l'interprétation des données collectées, avec lesquelles les différentes équipes espèrent décrire de nouveaux phénomènes sur les lacs.

2. Summary

The Leman-Baikal project is an international Swiss-Russian collaboration that investigates lakes surface properties using ultralight aircrafts. The primary objective is to compare the water quality and the energy balance of Lakes Leman in Switzerland) and Baikal in Southern Siberia region of Russian Federation. Remote sensing from ultralight aircrafts allow to map the spatial heterogeneity of these properties at a high resolution, which are particularly interesting for land-water interfaces in lakes.

This multidisciplinary project regroups different laboratories within EPFL and teams from Baikal Institute for Nature Management and Lomonosov Moscow State University. Four EPFL laboratories (TOPO, LASIG, APHYS, ECOL) are focussing on remote sensing to map chlorophyll a, total suspended matter, dissolved organic carbon and temperature in surface water of both lakes. Three laboratories (WIRE, EFLUM, CRYOS) in collaboration with Princeton University are investigating turbulences at the air/water interface on Lake Leman.

After a testing phase in 2013, the remote sensing platform was improved and successfully collected multispectral and hyperspectral observations above lake surfaces. In 2014, 17 flights took place above Lake Leman during 3 campaigns in February/March, April/May and September. The flights focussed on the mouths the Venoge and Rhône Rivers, where mixing of waters from different qualities showed interesting patterns. To obtain a more global view, we also covered the entire Lake Leman.

On Lake Baikal, we collected multispectral and hyperspectral observations on the entire Selenga Delta in August 2014. The delta showed an incredible diversity of plants, forests, water channels and stagnant water bodies that was well captured by our images. The success of this campaign was ensured by the collaboration with Russian students implicated in the project.

Data processing of the massive dataset will soon deliver the first maps of water qualities. The remote sensing and the ground truthing teams are working together on the last step of a long process chain. However, iterative steps are still needed to ensure a high data quality of the results. To further interpret data from the Selenga Delta, four Russian students will spend internships at EPFL starting mid-November. We therefore expect that results will soon assess the heterogeneity of water quality on both lakes at a higher spatial and temporal resolution than ever achieved.

Concerning the atmospheric boundary layer, turbulences were measured during the first two campaigns on Lake Leman. However, the ULM platform revealed to be insufficiently adapted to atmospheric measurements due to vibrations. In addition, meteorological conditions with high wind velocities, that would be the most interesting, were too dangerous to handle with a ULM.

In 2015, the remote sensing teams plan to collect additional data on Lake Leman during a last campaign in April/May. Another campaign along the entire coastline of Lake Baikal is planned in July and August 2015 in close collaboration with Russian colleagues. This year, the focus will be on the interpretation of the collected data, with which the different teams hope to describe new findings on lakes.

Table of Content

3. Remote sensing platform – TOPO / LASIG laboratory

Dr. Y Akhtman, D Constantin, Prof. B Merminod, Prof. F Golay, M Parkan, M Rehak, Dr. D Tuia

3.1. Methodology

The main principle of the research methodology is constituted by the concurrent acquisition of airborne wide-area and surface point-based data as illustrated in Figure 1. Specifically, we have employed an ultralight aircraft in order to carry an airborne remote sensing platform, and a boat equipped with a range of sensors and water sampling equipment.

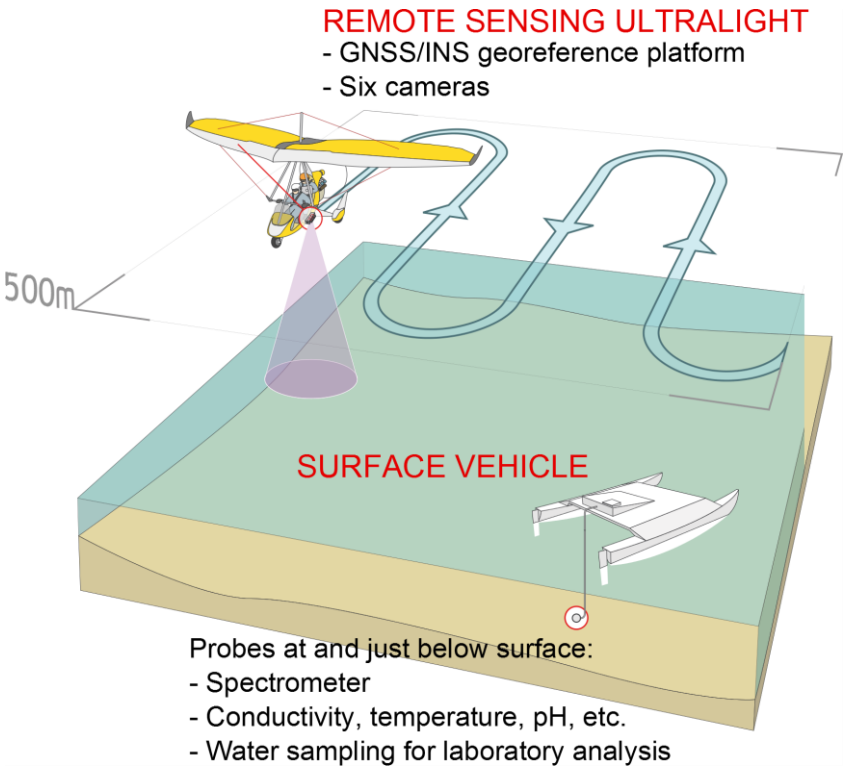

Figure 1: Concurrent airborne and surface collection of data

As part of the Leman-Baikal project, a remote sensing platform was developed to collect multispectral and hyperspectral observations of both land and water surfaces from ultralight aircraft. The platform is comprised of six cameras, auxiliary position and orientation sensors, as well as data recording equipment. Our main instrument is constituted by a Headwall Photonics Micro Hyperspec VNIR sensor. In addition, the platform includes the following cameras: 5MP RGB, 1.3MP Panchromatic camera, 5MP Near-Infrared, a 16 band, 2MP hyperspectral VISNX prototype as well as a thermal infrared sensor based on a FLIR Tau camera. The resultant remote sensing platform is portrayed in Figure 2. As our airborne carrier we have used an Air Creation Tanarg ultralight aircraft.

Figure 2: Our most recent iteration of the hyperspectral system next to a 2 Euro coin (left) and our airborne carrier, the Air Creation Tanarg ultralight (right).

The surface-based samples were used to produce a detailed characterisation of the water properties at sampling locations. Additionally, the reflected spectral response of the water surface at each sampling point is registered. The reflectance properties are correlated with the various water characteristics and the spectral response-based indicators for the various chemical and biological water properties are derived. The resultant spectral signature-based indicators are subsequently utilised in order to derive a wide-area maps of water properties using the multispectral and hyperspectral data collected with the use of the airborne remote sensing platform.

In this context, the concurrent airborne and surface based data acquisition methodology exemplified in Figures 3 and 4 is essential for the sake of calibration of the airborne data, as well as the analysis of data quality, accuracy and precision. Correspondingly, ground sampling sites were chosen within the trajectories of the aircraft where the strongest variability of water quality parameters could be observed. We used three radiometers to validate the hyperspectral acquisition from the ULM: the OceanOptics USB 2000+, the waterInsight WISP 3, and the Ramses TriOS system. In addition, water quality parameters were measured with a Seabird CTD19+V2 for chlorophyll-a and turbidity and sub-surface water samples for dissolved yellow substances. These latter parameters are used as supervision in a neural network which interprets the ULM hyperspectral data in terms of water constituents.

3.1.1. Data acquisition

Adding to the 7 Terabytes of data collected in 2013, we have acquired another 8 Terabytes of hyperspectral, RGB and thermal data, covering more than 13000km of flight tracks, while also including more than 100 in situ sampling sites. The hyperspectral image resolution was around 0.5 m/pixel, giving us very high resolution spectral maps of our areas of interest.

The 2014 campaigns were carried out over Lakes Leman, Baikal and Gusinoe. Our main areas of interest were:

- A scan of Lake Leman, to obtain a complete map
- Lausanne area, to assess impact of human activity on the lake
- Rhone delta, to study sediment dynamics
- Selenga Delta in Baikal, due to its biological and water dynamics

- Lake Gusinoe near Ulan Ude, to assess the impact of heavy metal pollution from exploded ammunitions

Since 2013, the end of the last campaign, we have significantly streamlined our remote sensing platform, while improving its quality. Due to the great size of the areas we have to cover in the scope of this project, we had to redevelop most of the remote sensing platform from scratch, rebuilding everything from sensor integration to data processing software and user interface. Weighing around 3 kg and being completely autonomous, it is the most compact and easy to use platform of its kind. This work has allowed us to cover larger areas more effectively, reducing the time required to prepare the flights as well as lowering the data volume, all-the-while improving the spectral quality of our images.

Lake Leman phase

The first step of the Leman Phase was mainly centred on testing and calibrating the new system. As a consequence, most flights were carried out in the same areas as in 2013, in order to compare quality improvements as well as the variation in time of our areas of interest such as Vidy Bay, Venoge Delta, Rhone Delta and the Lausanne shoreline.

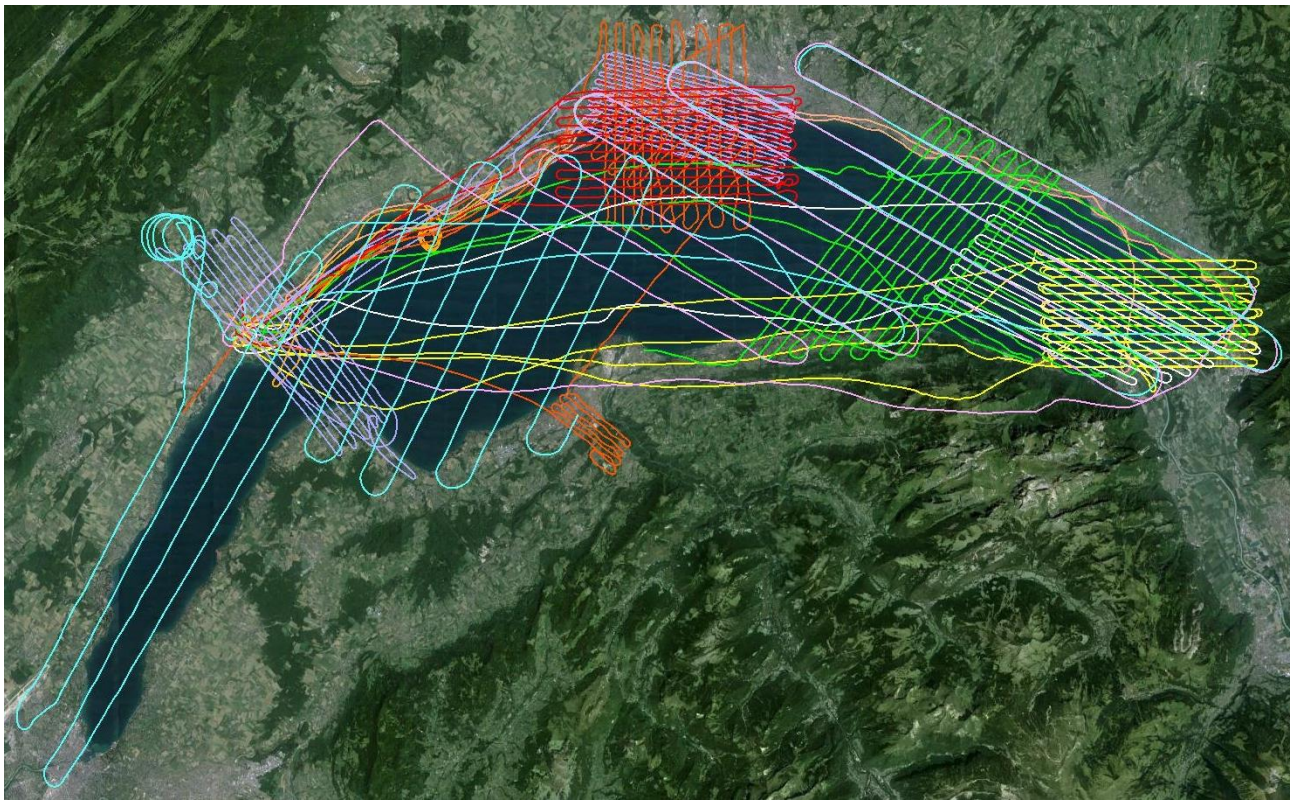

Figure 3: Leman campaign spring 2014

The data collected on Lake Leman was especially helpful in debugging and optimizing our system for the much larger data acquisition in Baikal.

Date	Time	Location	Altitude	Measurements
20-02-2014	10:00-11:07	Gland-Rolle shoreline	1000 m	Calibration + HSI
07-03-2014	08:30-11:30	Rhone delta	1500 m	HSI, RGB, Thermal
07-03-2014	13:30-16:30	Rhone delta	1500 m	HSI, RGB, Thermal
10-03-2014	09:00-13:30	Morges-Lausanne shoreline	1000 m	HSI, RGB, Thermal
10-03-2014	14:30-16:45	Gland-Yvoire narrow	1200 m	HSI, RGB, Thermal
12-03-2014	08:30-12:00	Morges-Lausanne shoreline	1500 m	HSI, Thermal
12-03-2014	14:00-16:30	Morges-Lausanne shoreline	1000 m	HSI, Thermal
10-04-2014	09:30-13:00	Rhone delta	3000 m	HSI, Thermal
17-04-2014	08:00-12:00	Leman Lake East	4000 m	HSI, RGB, Thermal
05-05-2014	08:30-12:00	Leman Lake East	4000 m	HSI, RGB, Thermal
05-05-2014	13:15-16:30	Leman Lake West	4000 m	HSI, RGB, Thermal
11-09-2014	10:00-11:30	Gland-Rhone Delta shoreline	1000 m	HSI, RGB, Thermal
16-09-2014	10:00-12:30	Rhone delta	1500 m	HSI, RGB, Thermal
16-09-2014	15:00-17:00	Lake area between Evian-Les-Bain <-> Chexbres	1500 m	HSI, RGB, Thermal
26-09-2014	10:00-12:30	Venoge Delta	1000 m	HSI, RGB, Thermal
26-09-2014	13:00-17:30	Venoge Delta and Thonon-Les-Bain area	1000 m	HSI, RGB, Thermal
11-09-2014	10:00-11:30	Gland-Rhone Delta shoreline	1000 m	HSI, RGB, Thermal

Table 1: Flight details of 17 flights over Leman Lake, carried out in February-May 2014

Lake Baikal phase

In the next phase of the project, taking place between 25th July and 20th August 2014, we carried out a comprehensive field campaign over the Selenga River delta in the Southern Siberia region of the Russian Federation. The campaign was conducted in close collaboration with the Geography Faculty of the Moscow State University and the Baikal Institute of Nature Management in Ulan Ude. Our airborne observations were complemented by extensive ground work, which included the collection and analysis of in situ samples for chemical properties, as well as the recording of the corresponding spectral reflectance signatures of the water surface.

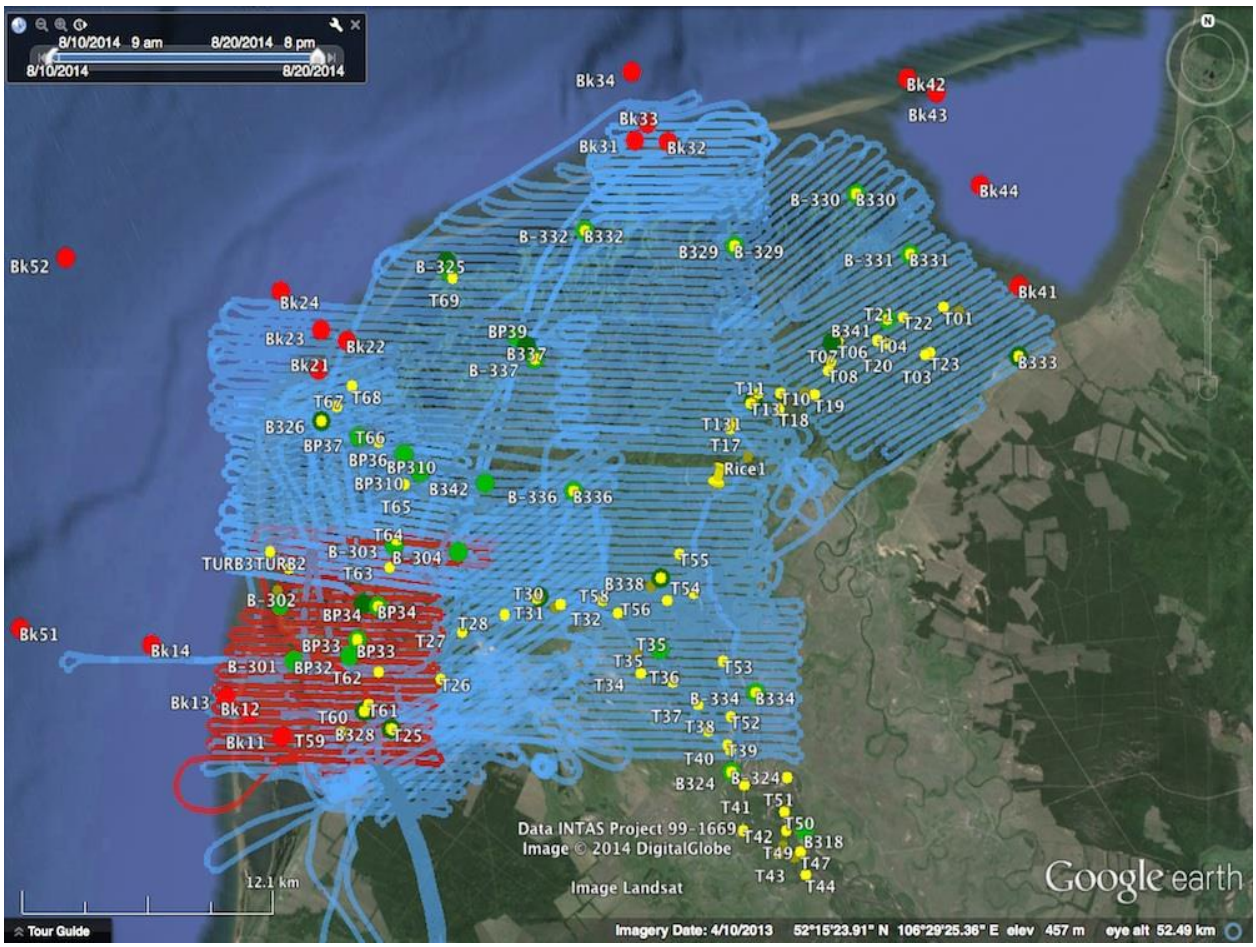

Figure 4: Baikal campaign 2014, complete scan of Selenga Delta and ground control points.

As our upgraded system allowed us to assess the quality of the data acquired in real-time, all flights correspond to high quality data, covering the entire surface of the Selenga delta.

During the Baikal phase, we also acquired data with a second hyperspectral prototype system, jointly developed by our laboratory and the VISNX startup. While this new system is of lower spectral quality than the Headwall hyperspectral system, it presents multiple advantages as it is a highly miniaturized snapshot spectral camera.

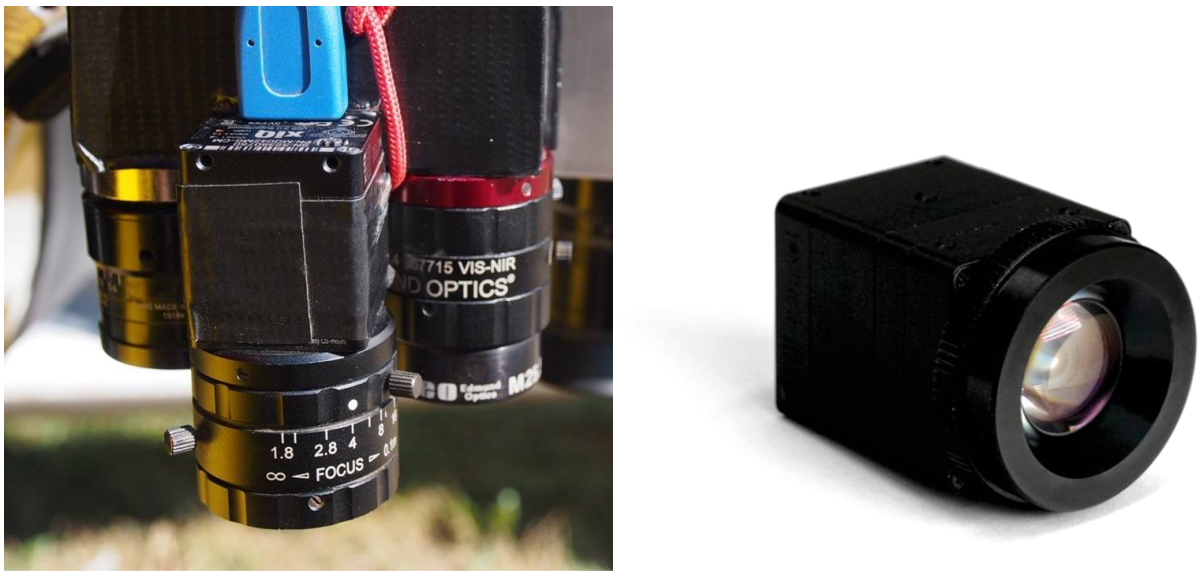

Figure 5: The VISNX hyperspectral camera prototype

The prototype system was tested alongside the main hyperspectral system and worked perfectly for all 100 hours of recording, producing more than 500,000 images.

The Baikal phase was continued with a week of data acquisition over and around Lake Gusinoe, where both systems performed very well.

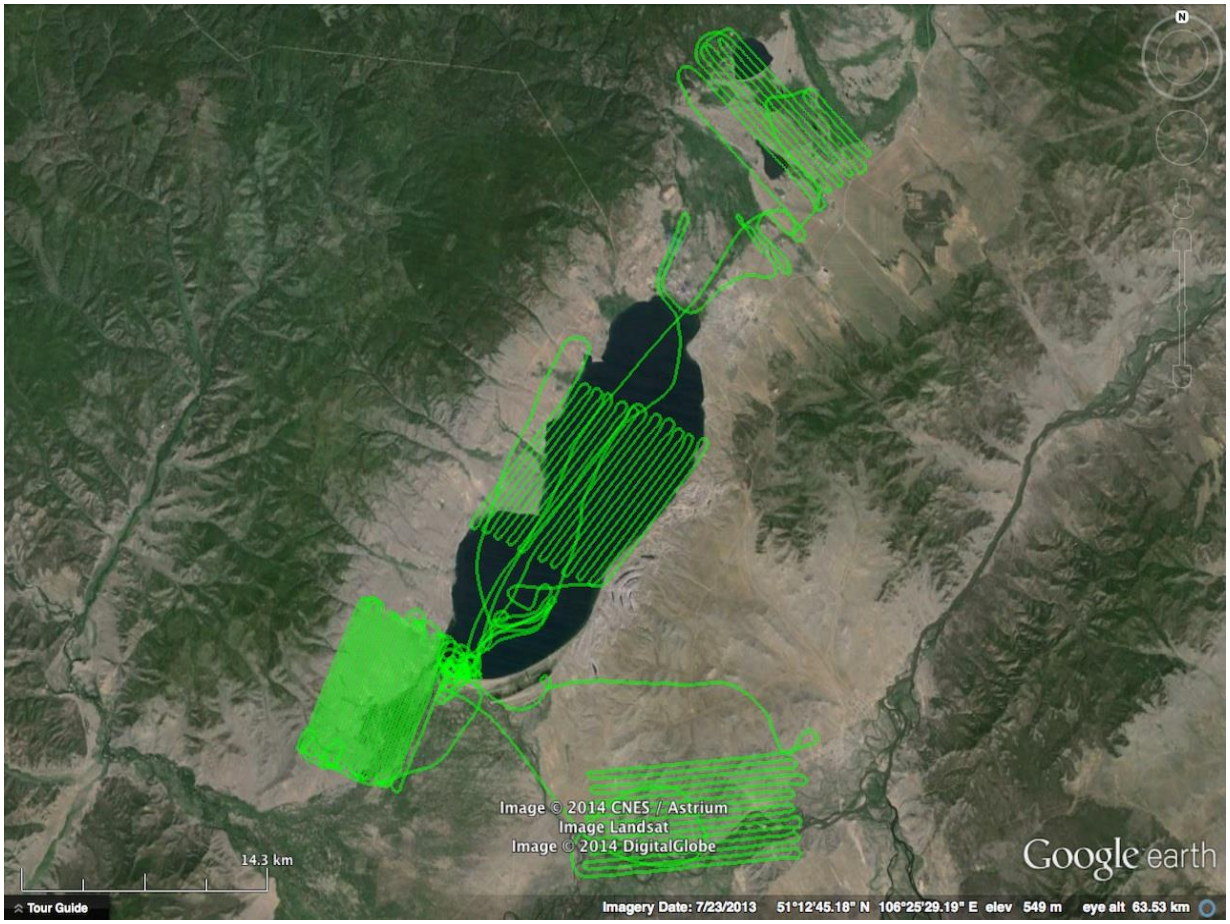

Figure 6: The campaign on Lake Gusinoe, August 2014

3.1.2. Data processing

The remote sensing data processing chain is being actively developed for the effective analysis of the material collected in the course of the various phases of the field campaigns. The raw data covered multiple data types including multispectral image sequences, hyperspectral line scan sequences, as well as auxiliary navigation data logs. The aim of the data processing methodology is the production of a data management system, which will facilitate access to synchronised, calibrated, as well as time and space referenced multimodal data. For example, major steps that comprise the implemented hyperspectral data processing pipeline include:

- geometric and radiometric corrections of the individual scan lines that compensate for both lens- and sensor related radiometric and geometric distortions;
- atmospheric correction that accounts for the specific lighting conditions, as well as the effects inflicted by the downwelling and upwelling propagation of light through the atmosphere;
- evaluation of the surface reflectance from the irradiance that takes into account specular effects and mitigate sun glint;
- DTM-based orthorectification and georeferencing.

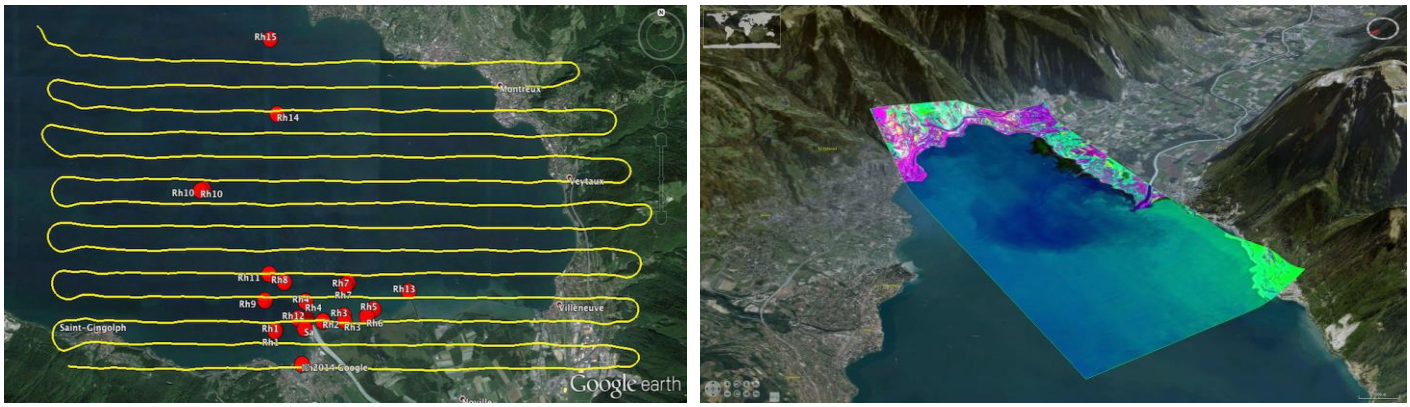

Figure 7: Data acquisition campaign of 7 March 2014 over eastern side of Lake Leman (left) flight trajectory (yellow) and in situ sampling sites (red); (right) three dimensional visualisation of the orthorectified and georeferenced hyperspectral data.

The performance of the resultant data processing chain is exemplified in Figure 7 that details the flight trajectory, ground sampling sites, as well as the corresponding hyperspectral data obtained on 7th March 2014 on the eastern side of Lake Leman. It should be noted, however, that not all stages in the detailed pipeline have been completed so far and its development remains a work in progress.

Furthermore, as part of the Leman-Baikal project we have developed and deployed a dedicated database system and a web-based GIS data management framework, which facilitates an effective and highly structured storage, search, retrieval and visualisation of multi-modal scientific data collected in the course of the field campaigns.

3.2. Preliminary results

We have conducted a range of methodological experiments, while collecting data from different altitudes between 500m and 4000m, resulting in the ground resolution of hyperspectral data of between 0.2-2 m/pixel.

Over Lake Leman the hyperspectral data shows particle dynamics clearly but also discriminates another element (in orange) that we assume is correlated with reflectance from lake bottom. Further data analysis is required to confirm these findings.

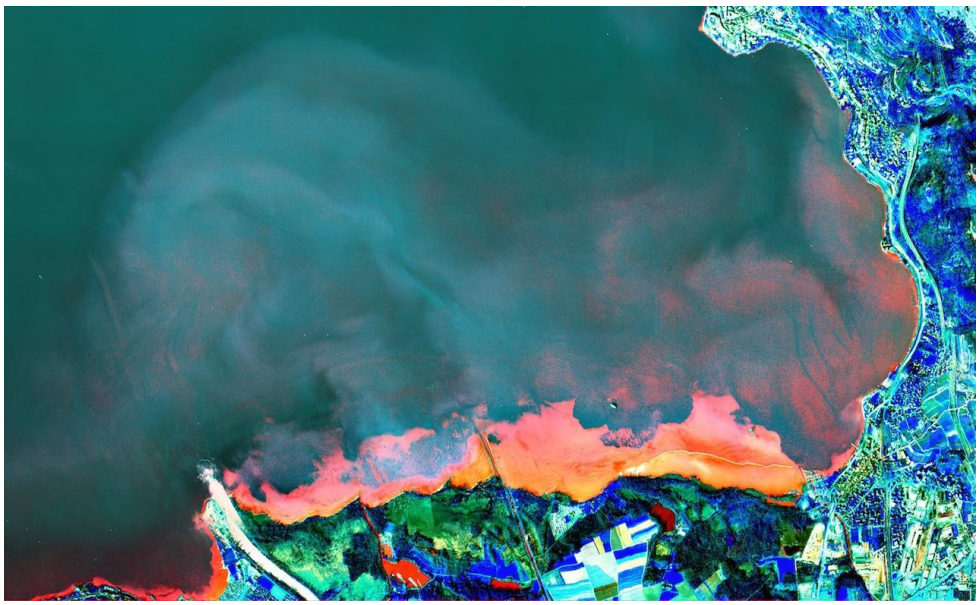

Figure 8: PCA of Rhone delta showing high discrimination between static waters and dynamic sediments

Over the Selenga delta, the hyperspectral images show high variance for various species of plants which are essentially green in RGB imagery.

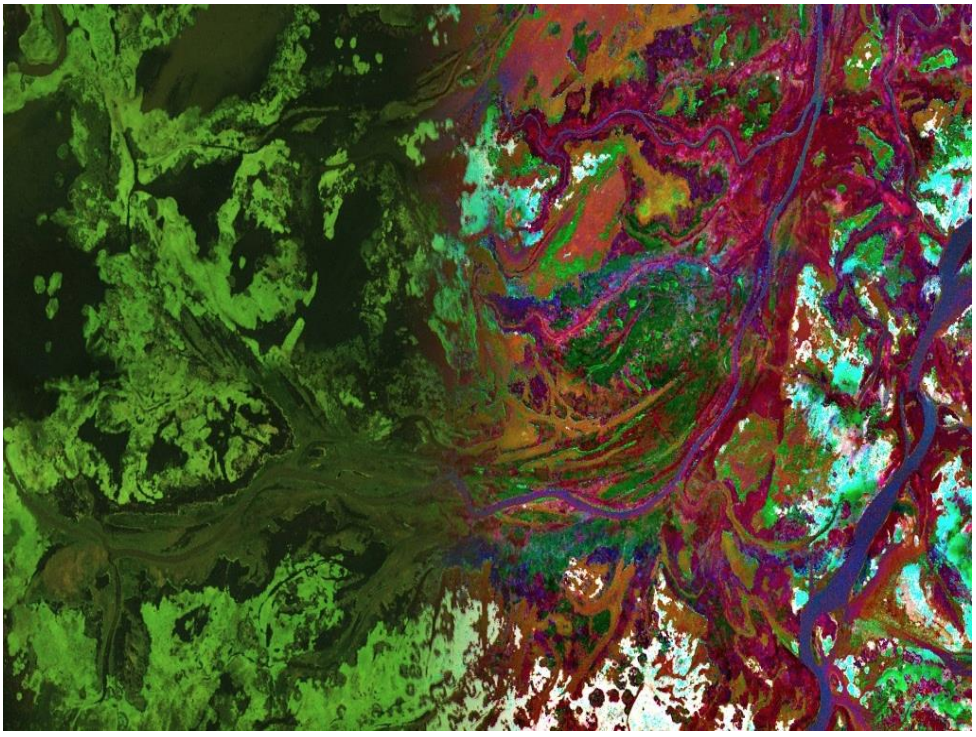

Figure 9: RGB to PCA transition of a hyperspectral image of Selenga delta.

Lake Gusinoe was an area of particular interest as several ammunition depots exploded after the Second World War and spread large amounts of toxic chemicals and heavy metals in the surrounding area and in the lake. While the RGB images show little discrimination of tainted soils, our hyperspectral images show strong spectral variation, especially around explosion sites.

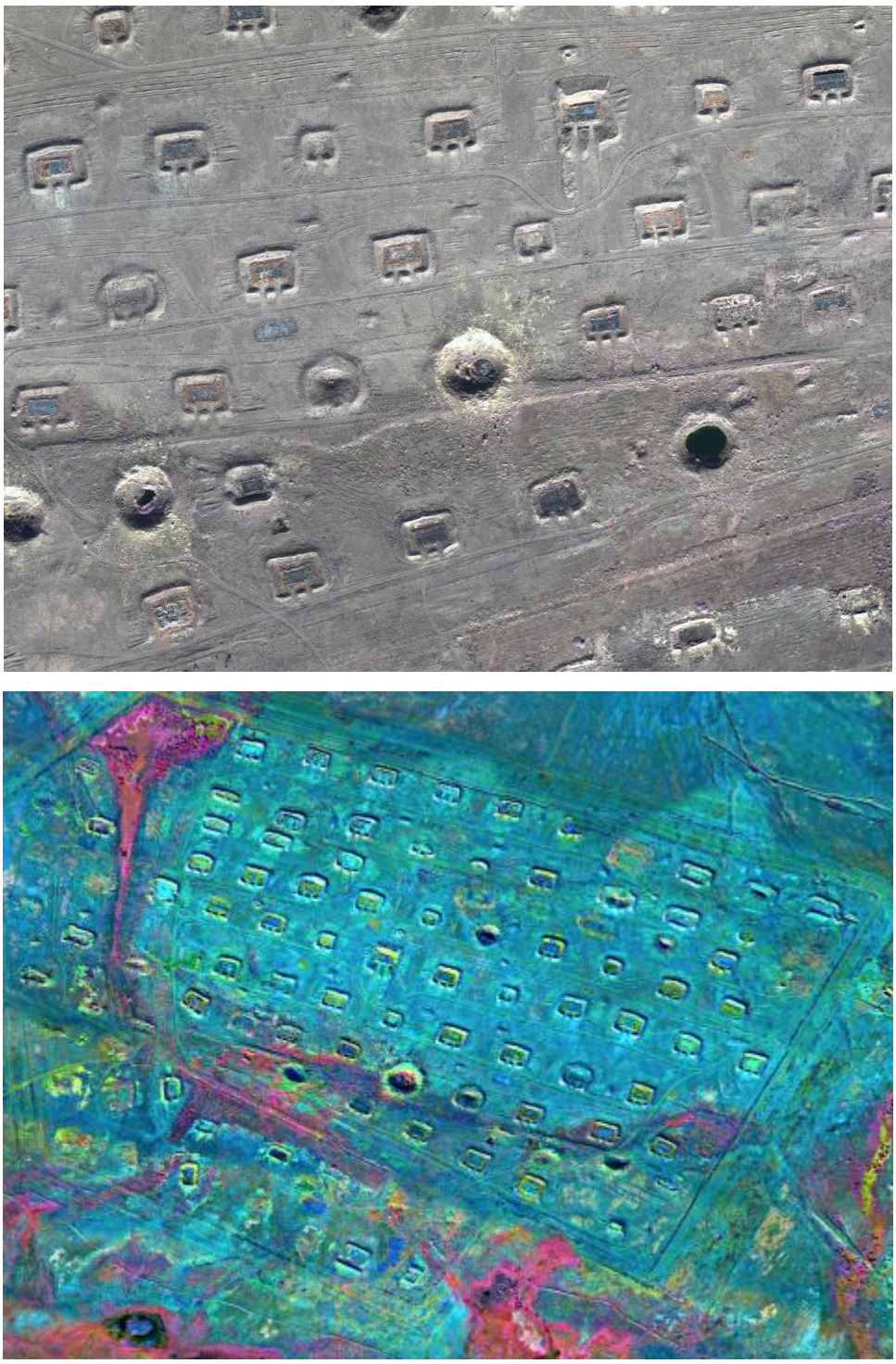

Figure 10: RGB and hyperspectral PCA images of ammunition depot sites

4. Thermal images – ECOL Laboratory

Prof. D A Barry, A Irani Rahaghi

The water temperature of freshwater lakes is mainly influenced by the surface heat flux. Temperature changes in turn affect the physical, chemical and biological states of the water body. The objective of ECOL laboratory within Leman-Baikal project is to characterize the variability of the lake surface heat flux. This investigation will be accomplished using available data, field measurements and a validated 3D

hydrodynamic model (Delft3D). The measurements include remote sensing and in situ data. The former comprise AVHRR[1] satellite data and ULM[2] surface thermal images, while the ECOL catamaran and a CTD profiler are used for ground truthing. Furthermore, an operational numerical weather prediction model, namely COSMO-2 (run by the Swiss meteorological service), will be used to obtain the spatio-temporal variability of meteorological data over Lake Leman.

4.1. In situ measurement: ECOL catamaran data

The ECOL catamaran is an autonomous platform (although legally operated with an accompanying boat) equipped with various sensors. All data – position (GPS), air and water temperature, net radiation, wind speed and direction, current profiles – are monitored and collected in real-time. An ADCP[3] is integrated when water current velocity profiles are of interest. In the 2014 ULM campaign, measurement tracks were chosen within the trajectories of the ULM, as well as in other areas of interest. Table 2 shows the summary of such measurement campaigns. Figure 11 shows a sample measurement path together with some monitored parameters. Regarding in situ data, the CTD profiles measured by/in collaboration with the APHYS laboratory will also be used for thermal investigation of both lakes.

Table 2: Summary of ECOL catamaran measurement campaigns over Lake Leman in 2014.

Date	Location (Starting point)	Measurements*
31.01.2014	Vidy Bay	WT, AT, WS, CNR4
11.02.2014	Vidy Bay	WT, AT, WS, WD, CNR4
07.03.2014	Vidy Bay	WT, AT, WS, WD, CNR4
10.03.2014	Vidy Bay	WT, AT, WS, WD, CNR4
12.03.2014	Vidy Bay	WT, AT, WS, WD, CNR4
10.04.2014	Vidy Bay	Navigation test
05.05.2014	Rolle	WT, AT, WS, WD, CNR4
19.05.2014	Rhone	ADCP
13.06.2014	Rhone	ADCP
26.06.2014	Vidy Bay	WT, AT, WS, WD, CNR4
16.09.2014	Lutry	WT, AT, WS, WD, CNR4

* WT: water temperature; AT: air temperature; WS: wind speed; WD: wind direction; CNR4: all radiation components

[1] Advanced Very High Resolution Radiometer
[2] Ultra Light Motorized
[3] Acoustic Doppler Current Profiler

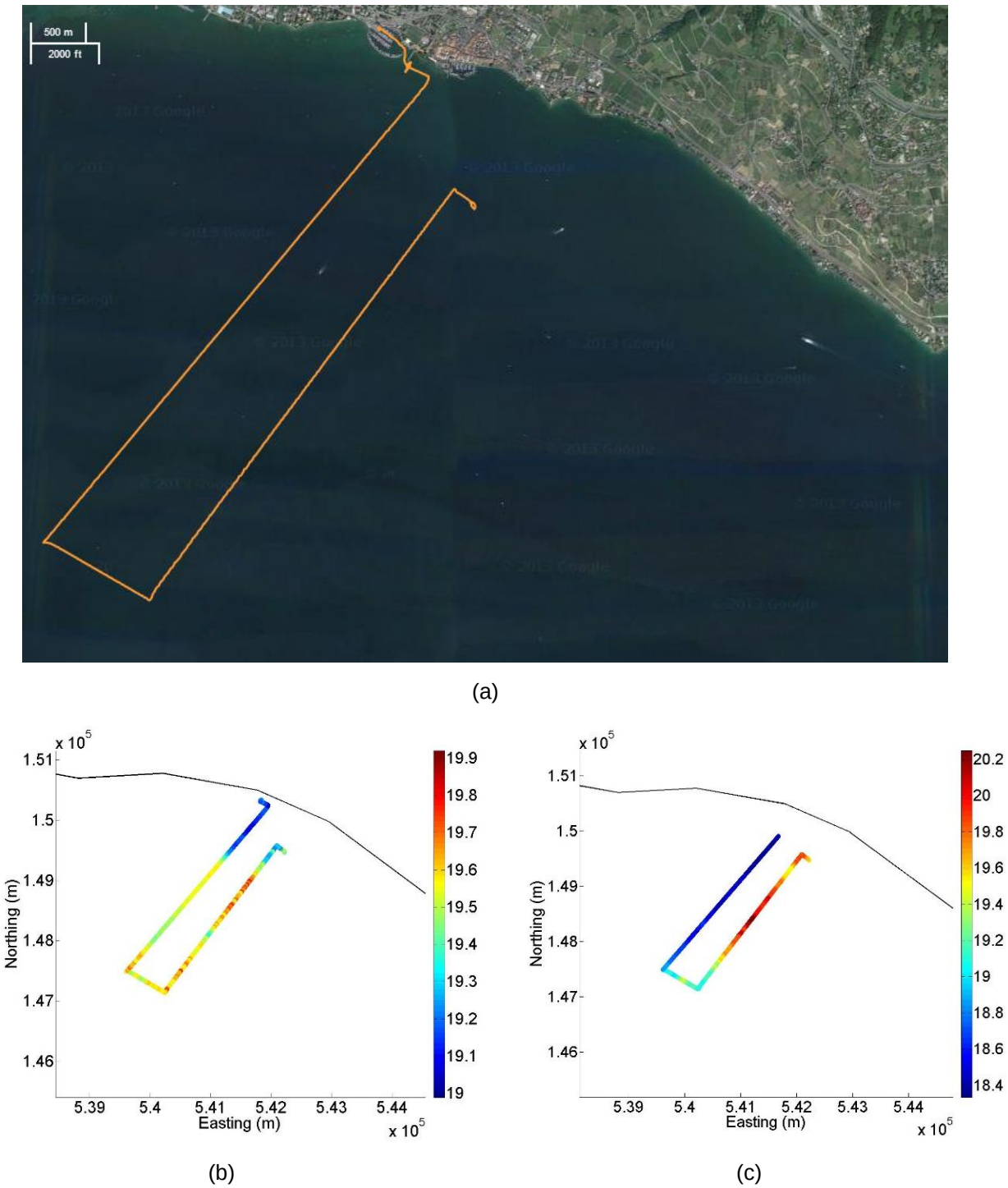

Figure 11: Example of the catamarn trajectory (a), corresponding near surface water temperature (b), and air temperature (c). The measurement was performed on 16 September 2014, between 11:51 to 14:07.

4.2. Primary comparison of ULM-Satellite data

We use different data sources for lake surface water temperature (LSWT), including remote sensing and in situ measurements. The latter have high accuracy but are at the point scale. The satellite images, on the other hand, have lower spatial resolution but cover large areas. The available satellite data might be suitable for detecting the large-scale thermal patterns, but not meso-scale or small scale processes. The key issue here is to gain the maximum benefit from all data sources, namely the accurate information

given by the sparse in situ profiles and the high resolution but less accurate LSWT satellite data. The data from different spatial supports thus need to be blended. The main objective of blending is to correct the large-scale part of the airborne fields using meso-scale (surface thermography) and in situ measurements in an optimal way. In the first step, synchronizing the captured thermal images and ULM navigation data is necessary. This issue was addressed during this year. Figure 12, for example, shows the ULM trajectory on 14th May 2013. For preliminary study of thermal images, ULM data were compared to satellite data on the same day. But, the raw thermal images contain artefacts (inherent of the instrument used) that must be eliminated. In an initial study, we assumed a constant error within all images. In other words, one image in a constant temperature zone within the satellite image was considered. Then, the difference between each pixel value and this reference temperature was assumed to be the pixel error. Finally, the average temperature of each corrected image was calculated. Figures 12 (b) and (c) show the comparison of selected thermal images and their corresponding error, i.e. satellite value minus image average temperature. Although the lake thermography trend in the selected path (along which data validation is carried out) is in a good agreement with satellite data, still the error is a bit high, and further or alternative corrections are needed. We will perform camera functionality quantification, artefacts elimination, image registration and data blending to achieve an upscaled LSWT field.

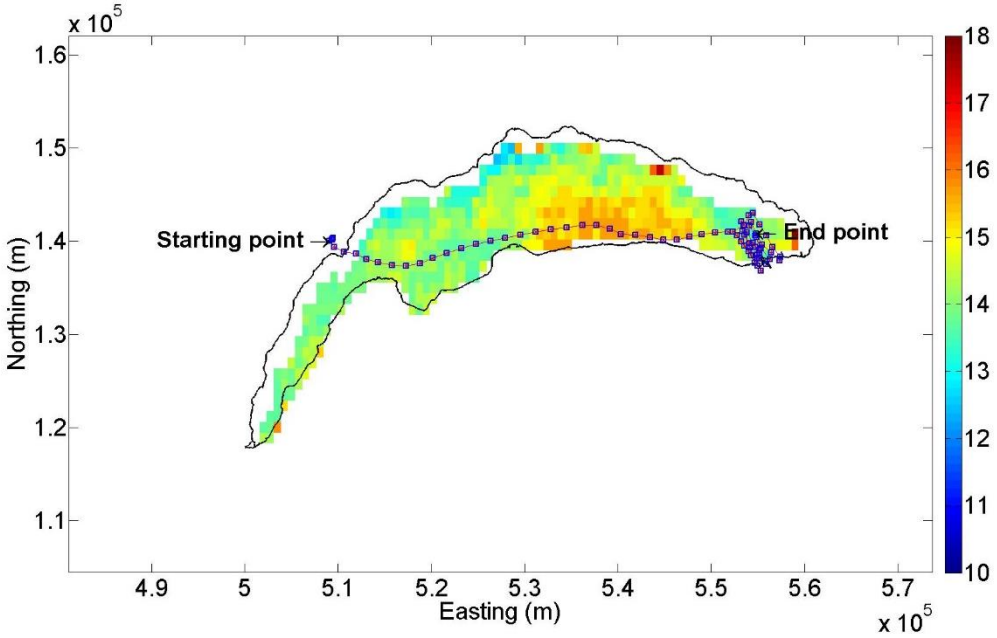

(a)

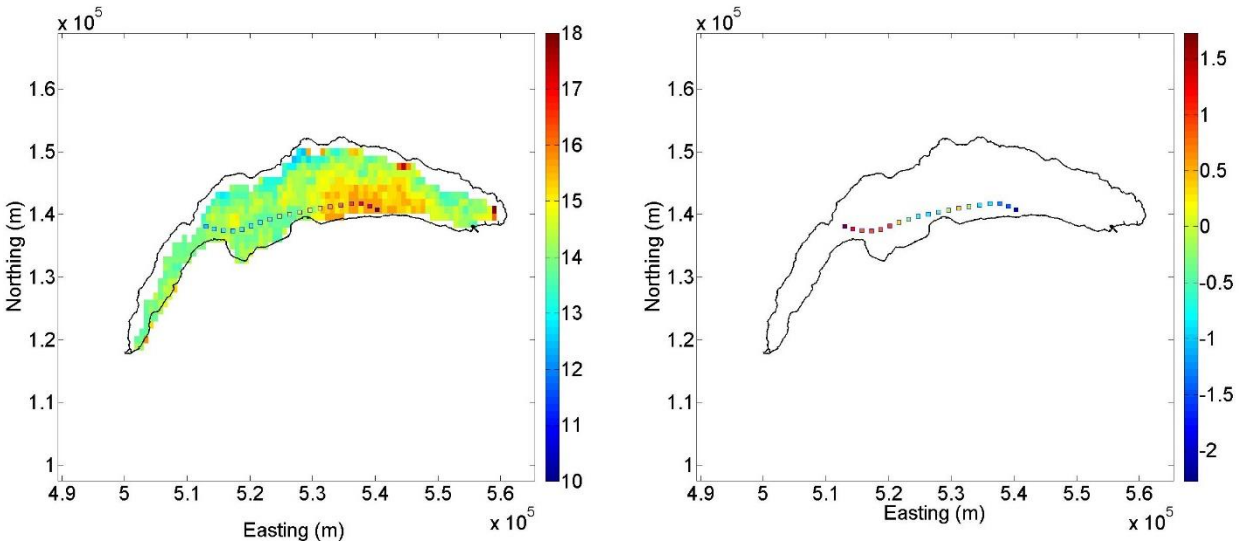

Figure 12: ULM trajectory and LSWT satellite data on the same day (a), comparison of the averaged image value and satellite data (b), and error with respect to this comparison

4.3. Bulk modelling of the lake surface heat flux

The lake surface energy exchange depends on several factors, making it difficult to estimate. The total heat exchange at the air-water interface is as follows:

$$Q_{tot} = Q_{sn} + Q_{an} + Q_{br} + Q_{ev} + Q_{co} + Q_{Pr} + Q_{Io} \quad (1)$$

The right side terms describe solar shortwave radiation, infrared radiation emission from the sky, surface reflection, evaporation/condensation, convection, precipitation onto the water surface, and the effect of inlet/outlet water, respectively. These terms are defined as positive when directed into the water. In the total heat balance of lake, the geothermal heat flux can influence the water temperature in deep zones. Since it is typically very small, around 0.1 W/m^2, its effect can be neglected. Furthermore, because of high flushing time[4] of large fresh water lakes (around 11 yr and 330 yr for Lake Geneva and Lake Baikal respectively), the throughflow heat flux is negligible. It must also be noted that the changes in LSWT during rainy days are usually due to changes in Q_{br}, Q_{ev}, and Q_{co}. Therefore, we can neglect the effect of precipitation and throughflow in the heat flux modelling of large lakes. As a result, only five major heat flux terms are considered.

We employed several bulk formulas for each heat flux term to estimate Lake Leman's total surface heat flux. They include 3 formulas for Q_{sn}, 3 formulas for Q_{an}, 3 formulas for Q_{br}, 4 formulas for Q_{ev} and 3 formulas for Q_{co}. Moreover, there are, in total, 6 calibration factors within the chosen formulas. The combination of different surface heat flux terms leads to a surface heat exchange model which requires various data. Meteorological data were taken from COSMO-2, while satellite imagery was used for LSWT. In order to find the best combination of the bulk formulas and to calibrate the model, the temporal evolution of the heat budget was estimated using long-term temporal series of vertical temperature profiles. Vertical temperature profiles at two

[4] Ratio of water volume per outflow

points, one in the Lake Geneva's large basin (SHL2 in Fig. 13 a) and one in its small basin (GE3 in Fig. 13 a), were used. Finding the best model for lake surface heat flux requires a comprehensive sensitivity analysis. However, two examples of temporal evolution and spatial variation of Lake Geneva heat budget are shown in Figures 13 and 14. Variability analysis of the obtained results will then be performed to specify the key factors underlying surface heat flux changes.

4.4. Numerical modelling

The temperature field is a scalar indicating the thermal energy field in lake. It obeys the general transport equations, called Navier-Stokes equations in the literature, which contain diffusion, advection and source terms. The Coriolis effect must also be taken into account for large lakes. In this project, Delft3D will be used to calculate velocity field and thermal structure in large lakes. The blended LSWT field and measured vertical temperature profiles can be used to calibrate the 3D model. The outcomes of this part include improved thermal and hydrodynamic modelling of Lake Leman via large-scale estimates of the surface heat flux, as well as the means to incorporate validated LSWT data from satellite imagery into real-time modelling and prediction of the lake hydrodynamics.

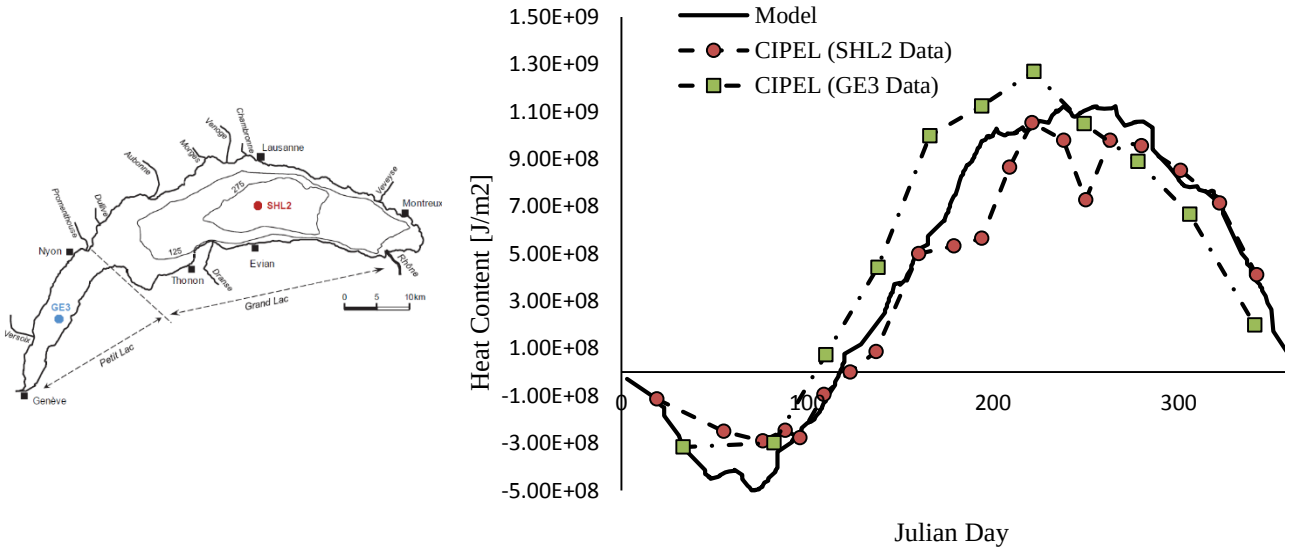

(a) (b)

Figure 13: SHL2 (coord. CH: 534.700;144.950) and GE3 (coord. CH: 506.100;128.040) monitoring points (a), the model results and monitoring points heat content for 2010 (b).

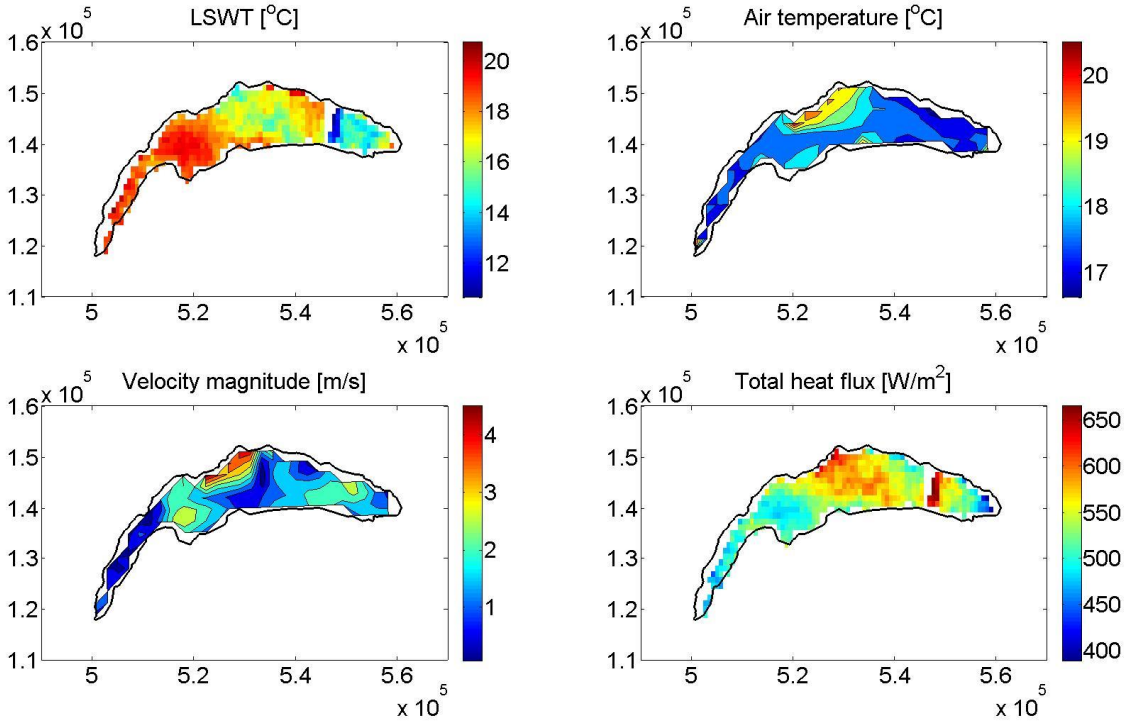

Figure 14: An example of bulk modelling of Lake Leman surface heat flux: LSWT (AVHRR satellite data), air temperature (COSMO-2 model), wind velocity (COSMO-2 model) and calculated total heat flux contours for 26 June 2010, 9 AM.

The Delft3D hydrodynamic model was applied to simulate Lake Leman's thermal structure in 2010. The meteorological data were taken from COSMO-2. The numerical results were obtained after performing preliminary sensitivity analysis on some influencing physical parameters such as Dalton number, Stanton number, Secchi depth, eddy viscosities and wind drag coefficients. Figure 15 (a) shows preliminary numerical results compared with observed data at one point (Buchillon, north shore of Lake Leman) for the whole period of simulation. In order to understand the capability of the current model in thermocline and deep water modelling, three different temperature profiles at SHL2 station were compared with model results (Fig. 15 b). It shows that the model performance is reliable at the thermocline and hypolimnion while the epilimnion requires more analysis and calibration.

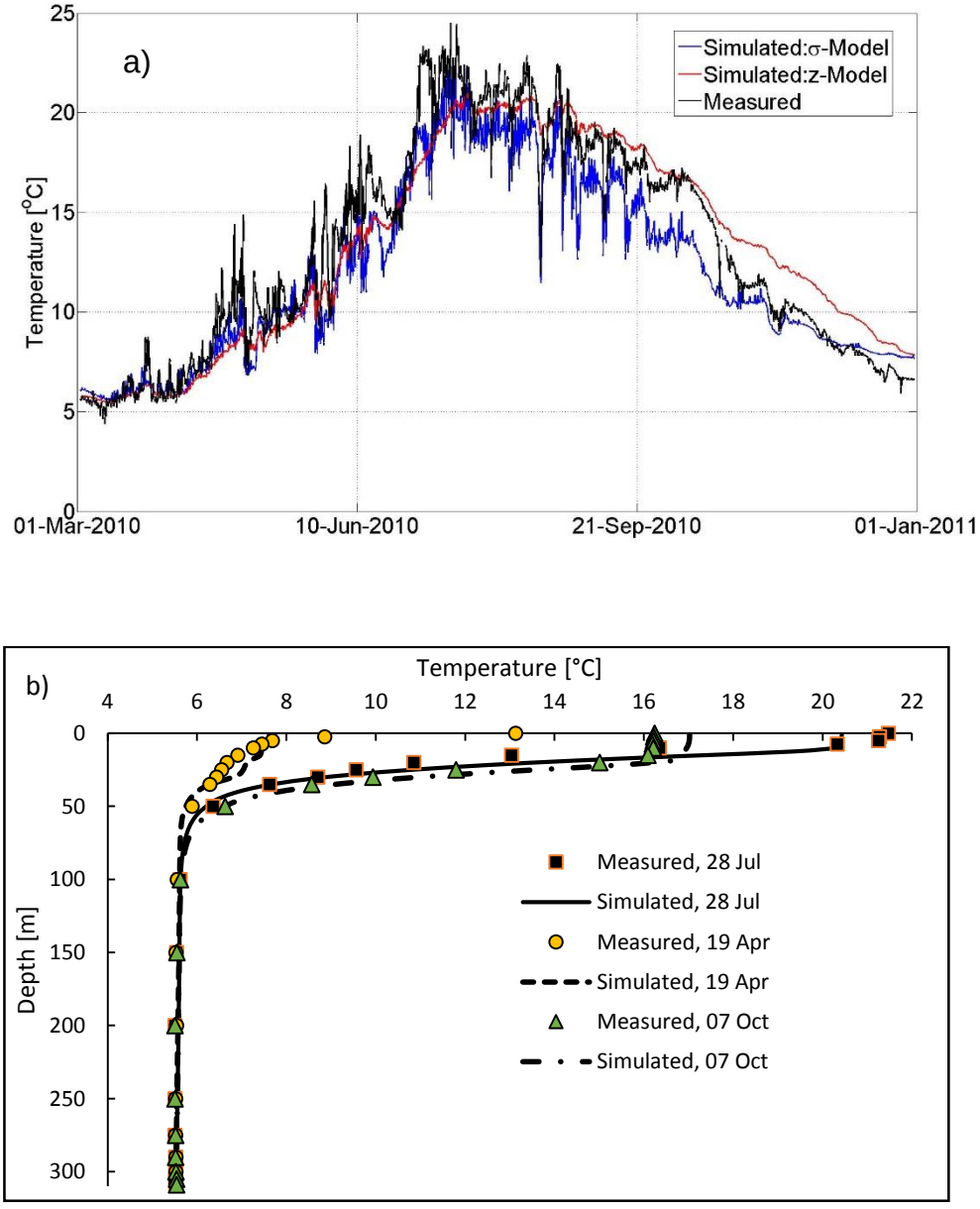

Figure 15: Comparison of the hourly near surface measured temperature (1 m depth) at Buchillon station with Delft3D models in 2010 (a), and comparison of observed and numerical vertical temperature profiles at SHL2 (b)

The methodology described above will, where feasible, be applied to data from Lake Baikal campaigns (validation to the degree possible for Lake Geneva is not of course possible):

- Having considered that the Lake Baikal surface thermography will measured with a drone in 2015, the obtained data can potentially be blended with point measurements and available satellite data, e.g. ArcLake data sets. It will provide a useful tool to investigate Lake Baikal surface water temperature patchiness as well as using them to estimate the lake surface heat flux.
- Measuring the meteorological data including wind forcing, air temperature and radiation terms together with surface and deep water temperature make it

possible to calibrate, and then estimate the total surface heat flux following the same procedure mentioned in section 4.4.

5. Water Quality - Margaretha Kamprad Chair (APHYS)

V Nouchi, Dr. D Bouffard and Prof. A Wüest

Hyperspectral systems on-board underwater vehicles, drones, and ultra-light aircraft are raising the interest of the remote sensing community to investigate processes with a spatial, temporal and spectral precision beyond spaceborne capabilities. These systems are particularly well suited for the water quality monitoring of *Inland Waters* because they allow the investigation of subtle variations in the spectral shapes of the targeted area with spatial resolution close to 1 m. This new generation of sensors is yet seldom used for the monitoring of water quality and our objective is to assess the suitability of such systems to accurately retrieve the IOPs (Inherent Optical Properties) and constituents of complex waters. The challenge is to validate the airborne observations acquired with new ultra- light hyperspectral cameras with ground truth references, physical model description and other better known hyperspectral sensors.

5.1. Methodology

The first approach is to develop an empirical model using Neural Networks (NN) to inverse the hyperspectral acquisition directly into constituent concentrations. In fact, the product of the image remains digital numbers from the raw signal of the camera and the model should be adapted according to the different steps of the processing mentioned below. To date, we elected NN because of their elasticity in terms of parameterization and because they are successfully used over complex waters (Doerffer and Schiller, 2007; Odermatt et al., 2010). To validate the acquisition and derived water quality parameters, we need to compare the estimations with reference measurements. The reference used can be left-over Ground Control Points (GCP) from the parameterization of the NN. We can also use CIPEL measurement in Lake Leman in combination with seasonal trends of Chlorophyll-a (Chl-a) concentrations derived from MERIS observation between 2002 and 2012. In particular, Isabel Kiefer identified which areas of the lake are well represented by CIPEL stations that we could further used for our calibration. Her work can also be used as a reference for the quality retrieval of IOPs and constituents from the previous generation of sensors. Concurrent observations from other airborne and spaceborne sensors such as World-View-2 (WV-2), RapidEye (RE), Airborne Prism EXperiment (APEX), HICO and possibly others will be used for radiometric as well as derived product performance references. The quality of the constituent retrieval will be a key parameter to evaluate the performance of the ultra-light system.

The calibration of ULM-acquisition allows to tune the model to increase the data-set. For instance the inter-scene calibration enables the use of several images in the learning set, in order to encompass a broader range of spectral variability in the learning process of the NN. The radiance estimation from spectralon measurements can allow the inclusion of band-ratio methods based on the ratio between impacting and exiting light from a water volume at particular wavelengths. Finally, the radiometric calibration of the camera will allow us to include optical properties and radiative-transfer models in the processing.

Regarding the model development to inverse the hyperspectral acquisition into bio-geochemical constituents, several water analyses were performed. The measured concentrations are the output to be expected from the model. To date, the measurements include Chl-a, Total suspended matter (TSM) and dissolved organic carbon (DOC) analysis from water samples, as well as turbidity, beam attenuation, temperature and fluorescence (Chl-a) measurement using a SeaBird CTD19+ V2 and/or a SeaSun CTD75M. The beam attenuation is the only measured IOP, but we should incorporate an extensive IOP measurement procedure in our framework because they constitute the physical link between biogeochemical contents and IOPs. However, such an analysis was performed once on Lake Leman during the spring bloom of phytoplankton in June 2014.

In addition to the biogeochemical analysis of the water, we performed radiometric measurements to validate ULM observations using a submerged TriOS Ramses (only on Lake Leman), an Ocean Optics USB2000+ and a Water Insight WISP-3.

5.2. Preliminary results

Since April 2013 four measurement campaigns were performed on Lake Leman with 19 sampled sites in spring 2013 and 131 sites in winter, spring and autumn 2014. Data were collected all over the lake with special focus on the Rhone delta and the Venoge river inflow (Figure 16).

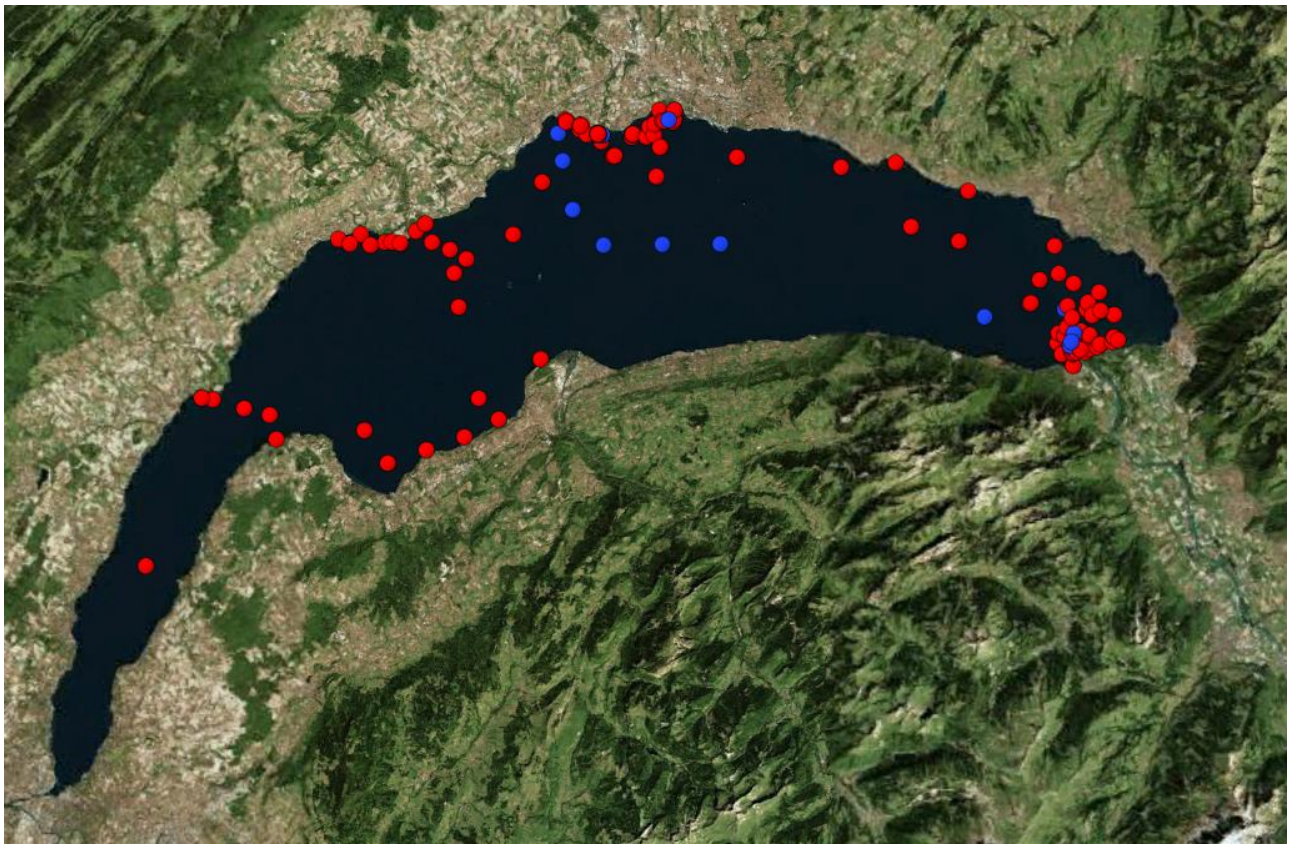

Figure 16: Ground control points performed in Lake Leman. The measurements collected in 2013 are blue and the one sampled in 2014 are red. Bing maps (source: pan-sharpened landsat-7 scene).

On Lake Baikal, 36 stations were sampled around and within the Selenga Delta in summer 2013. In August 2014, 78 stations were sampled mainly within the delta (Figure 17).

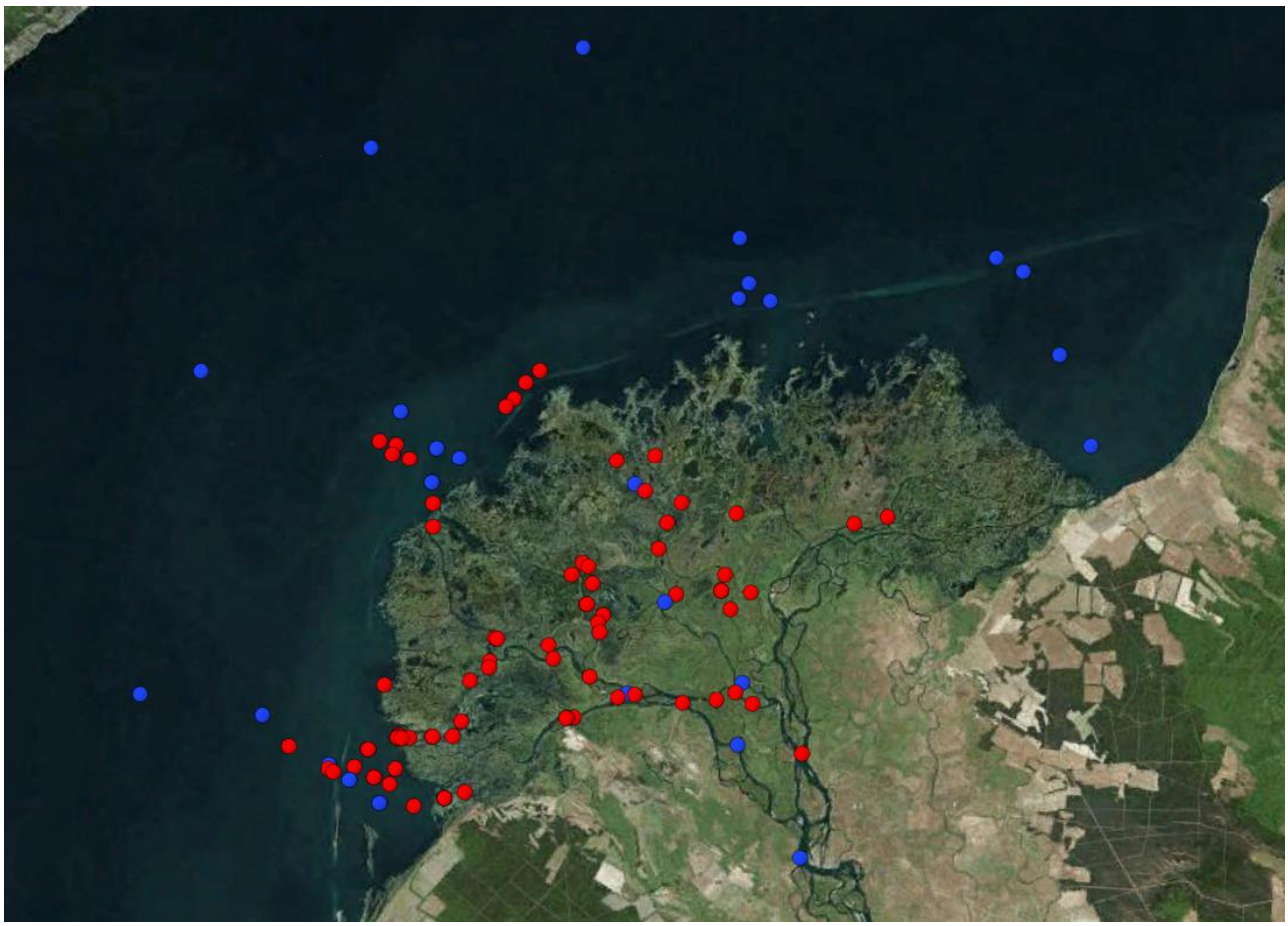

Figure 17: Ground control points collected in the Selenga Delta region of Lake Baikal. Bing maps (source: pan-sharpened landsat-7 scene).

The objective is to gather a maximum of Ground Control Point (GCP) representative of the different types of water in order to (i) feed the learning set for the statistical method we will apply, (ii) provide reference to validate the colour interpretation of the ULM-acquisition, (iii) implement physically-based model to enlarge the learning set but also to validate it. Figure 18 illustrates the ground truth strategy and shows different dots corresponding to the sampled sites. Their colour represents the amount of particles in the first 30 cm of the water column, which was sampled with a Sea & Sun CTD75M. Especially in the Selenga Delta, there is a large heterogeneity of channels in terms of size, currents and inter-connections, basin as well as fauna and flora, which lead to a high heterogeneity of water types. Thus, the aim was to access a maximum areas to correctly map the Selenga River inflow through the delta.

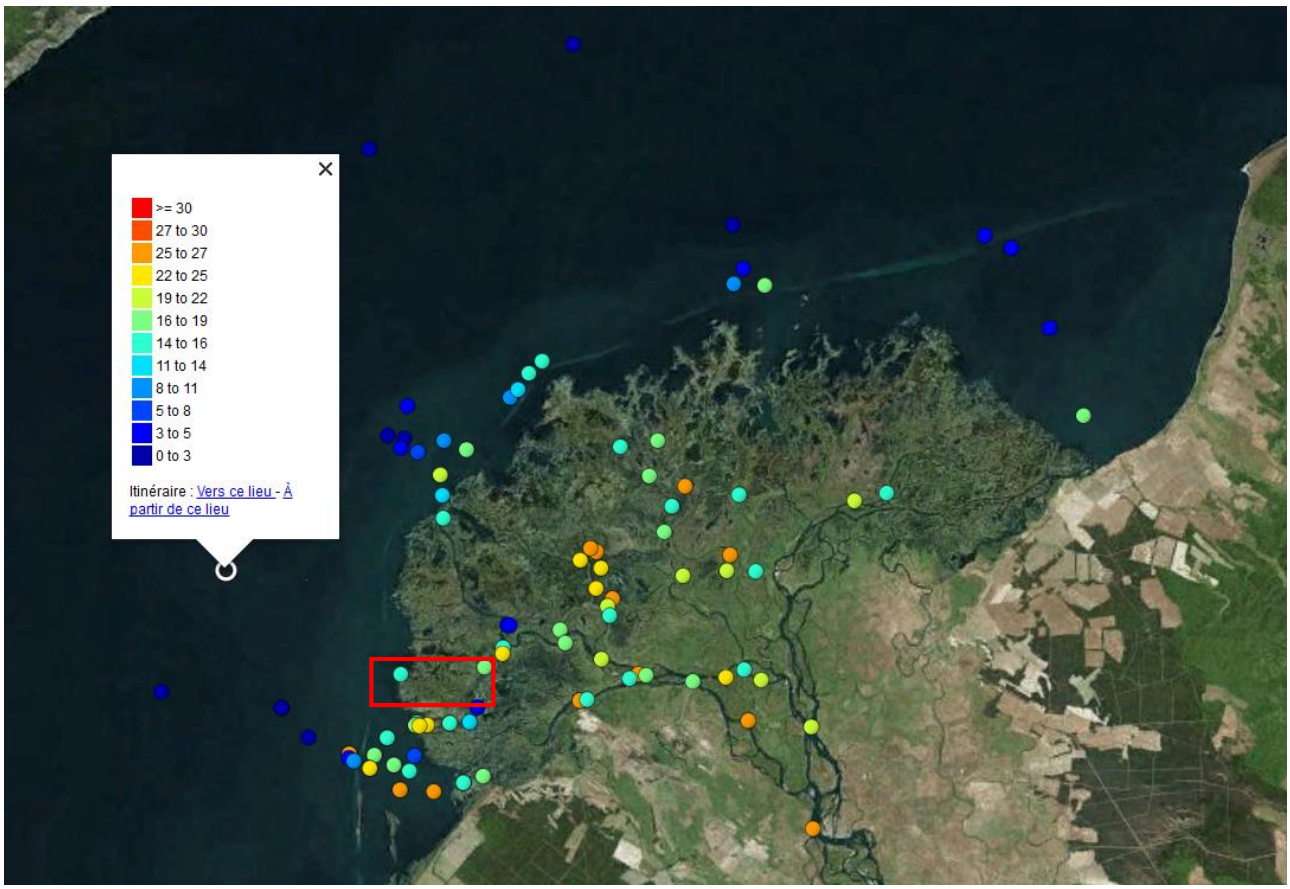

Figure 18: Particle distributions integrated over the top 30 cm of the water column sampled with a turbidity meter on a CTD in 2013 and 2014. The red square correspond to the area processed with the NN – see 'preliminary results'. Bing maps (source: pan-sharpened landsat-7 scene).

As introduced above, the first model we are developing uses a NN and a Multi-Layer-Perceptron in particular. The model is currently under development but a first glimpse of the results for both lakes is depicted in Figures 19 and 20 for the north-western part of the Selenga Delta and the Rhone Delta, respectively. On the grayscale images, dark pixels represent low particle concentrations and bright pixels high particle content. To date, the different substances observed are treated separately in the procedure and only the results from the TSM model are presented here. However, future models should incorporate all components in the analysis.

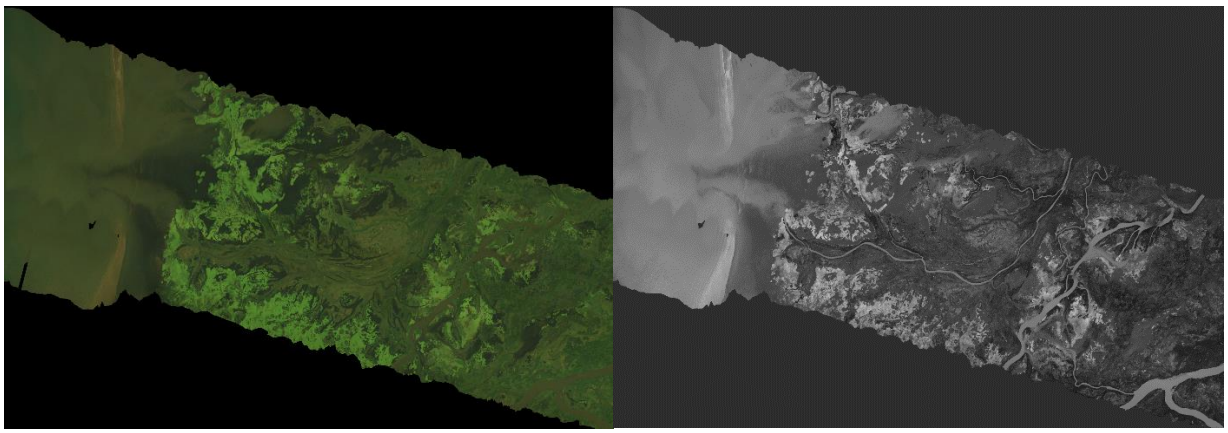

Figure 19: NN applied to an image located in the northern-western part of the Selenga delta. On the left is a RGB representation of the hyperspectral image and on the right is the particle concentration calculated by the NN. Acquisition on 04.08.2014.

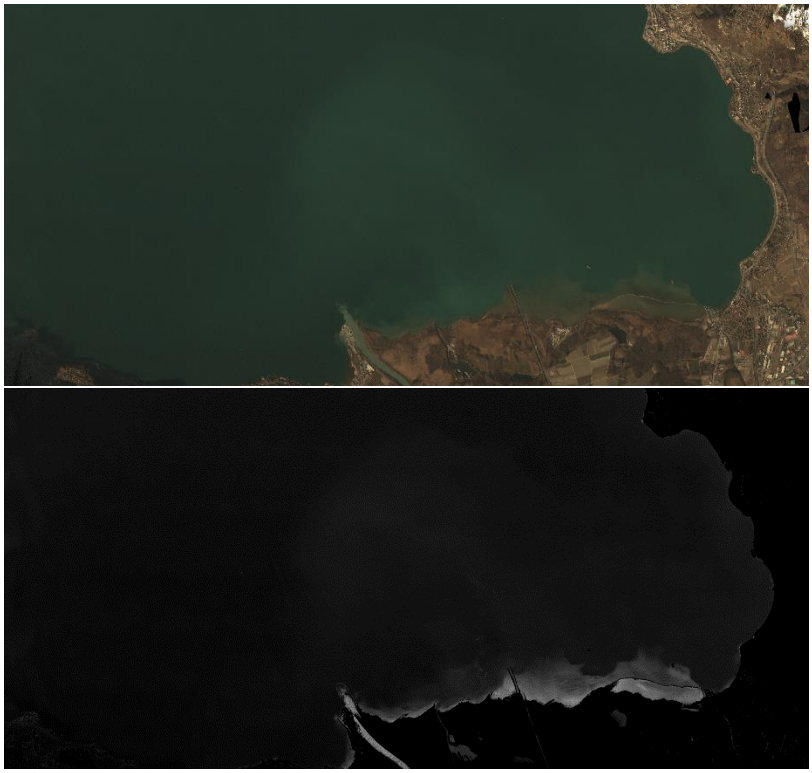

Figure 20: Same as Figure 19 for the Rhone Delta. Acquisition on 07.03.2014.

5.3. Perspectives

For next year campaigns on Lake Leman, we plan to investigate the diurnal variability in the Rhone region based on the approach adopted by Hunter et al. (2008). The high spectral and spatial resolution airborne sensor CASI-2 will acquire data during three flight on the same day over the same region in the morning, at noon and late in the afternoon. It allows the synoptic description of the spatial dynamics of the substances present in the water within a day and derive other bio-marker pigment than Chl-a from the extended spectral information.

The aim is to use two practical approach in Lake Leman and Lake Baikal to validate the acquisition of water quality data measured by ultra-light systems on-board small aerial platforms.

6. Atmospheric Boundary Layer measurements over Lake Leman with an instrumented ULM and wind LiDARs, WiRE

Dr. G.V. Iungo, N. Bocherens, F. Carbajo Fuertes, Dr. C. Markfort and Prof. F. Porté-Agel

6.1. Introduction

The Wind Engineering and Renewable Energy Lab (WiRE) of EPFL has contributed to the Lake Leman project through atmospheric measurements performed with an instrumented ULM and three ground-based scanning wind LiDARs. Two main measurement campaigns were carried out:

(a) Four day sessions of atmospheric measurements were performed with a ULM instrumented with two fast-response multi-hole probes, two total air temperature probes, one Pitot tube and two fast-response temperature sensors provided by Princeton. Simultaneous wind and turbulence measurements were made with three LiDARs. The main goal of the experimental campaign was to assess the considered experimental platform for atmospheric measurements.

(b) Three three-day field campaigns were performed using three LiDARs to measure the wake downwind of a tree canopy patch at the shores of Lake Leman. The days were chosen to capture a range of phenology cases, from no-leaf to full-leaf conditions. The primary goal of the experiments was to improve our understanding of how canopy density affects the wake structure downwind of a canopy patch at field scales.

6.2. ULM experiment

6.2.1. Experimental setup

Two fast-response five-hole pressure probes manufactured by Aeroprobe were installed on the ULM to perform 3D turbulence velocity measurements. The two probes were installed on a transversal boom attached to the ULM fuselage (Figure 21). The pitch angle was manually controlled by the pilot and measured through an inclinometer.

Figure 21: setup of the ULM.

Close to each turbulence probe the two fast response temperature probes provided by the Princeton team were installed. Moreover, at a distance of about 5 cm two total air temperature probes were deployed in order to measure a reference temperature needed for post-processing the data.

At one tip of the boom, a Pitot tube was installed in order to acquire a reference velocity. The Pitot tube was in turns connected to a SETRA transducer in order to measure the dynamic pressure.

All the probes were supplied by a 12 V battery installed on the ULM and recharged by an alternator connected to the shaft of the ULM propeller. The analog signals were acquired by a 16-channel CR-RIO, which was programmed and installed by the WiRE members. Finally the GPS-IMU unit IG 500 was installed in order to record during the flight the position, Eulerian angles, velocity and acceleration of the ULM.

All the software devoted to the data acquisition and monitoring of the tests during the flights was developed in LabView by members of the WiRE Lab.

6.2.2. Measurement procedures

Different types of tests were performed during the flights. The first test series was devoted to the ULM measurements through different flight paths:

(a) The first type of test was performed with the ULM flying at the maximum angle of attack for the given atmospheric conditions. A typical flight path is reported in Figure 22, together with the three velocity components measured. The goal of these measurements was the characterization of the vertical profiles of key atmospheric properties, such as mean wind velocity, turbulence intensity and mean temperature. The main drawback connected to this test path was the relatively large horizontal range covered during the flight. Indeed, by keeping a null yaw angle, significant horizontal distances were covered. Therefore, a certain spatial heterogeneity was detected through those measurements.

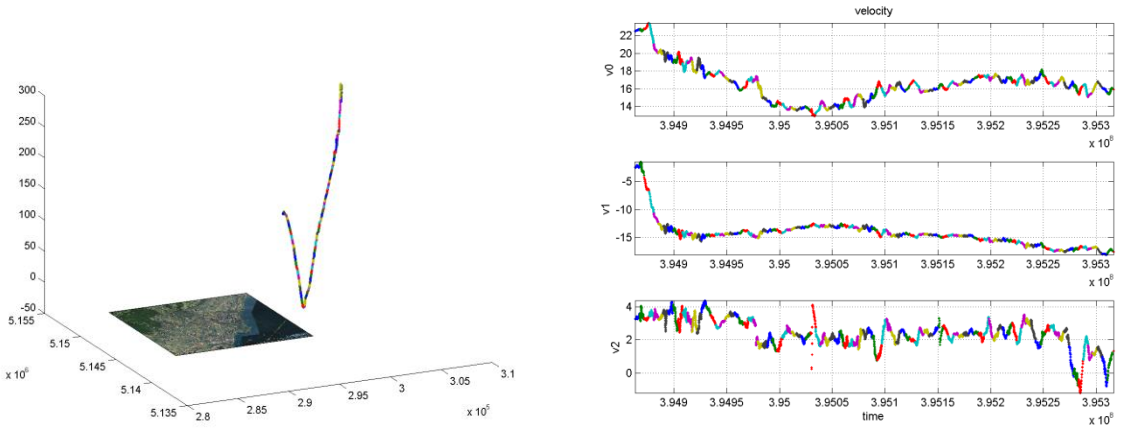

(a) (b)

Figure 22: Tests performed with the maximum angle of attack of the ULM: (a) flight path; (b) three components of the velocity vector.

(b) Another test series consisted of performing vertical measurements through spiral paths (Figure 23). For those measurements both yaw and angle of attack of the ULM were kept constant in order to gradually vary the height, but limiting the horizontal area spanned for the tests. Consequently, for those tests longer sampling periods were required to cover a certain vertical distance. The main challenge encountered with this measurement technique is represented by the data post-process. Indeed, the centrifugal force induced during the spiral path significantly affects the measurements and the correction of the data might not be accurate.

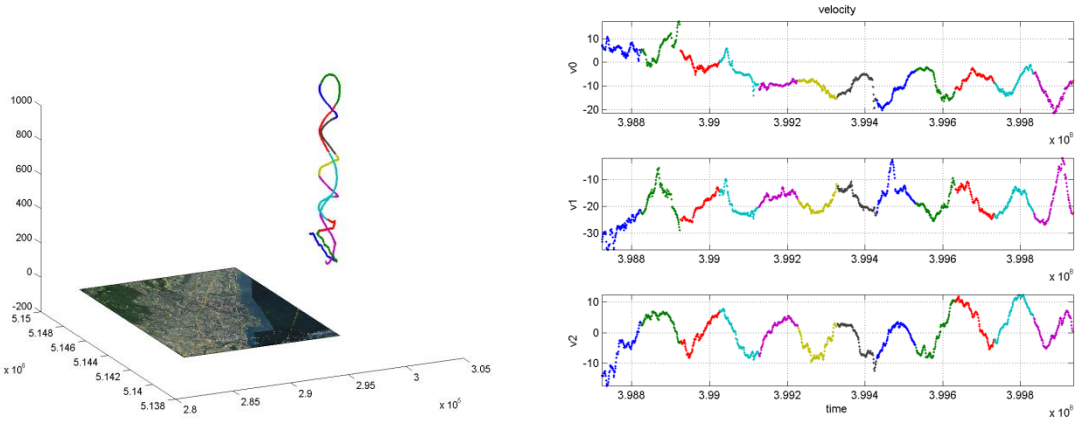

(a) (b)

Figure 23: Tests performed spiral path: (a) flight path; (b) velocity measurements.

(c) The last test series was performed by using circular paths performed at different heights. The goal of those measurements was to achieve a longer sampling period for each different height, thus producing more robust statistics.

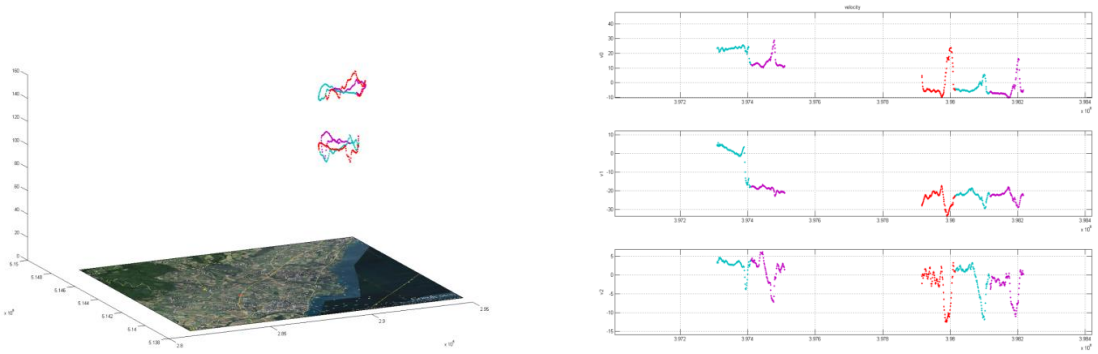

Figure 24: Tests performed with circular paths: (a) flight path; (b) velocity measurements.

6.2.3. Data post-processing

The voltage signals acquired through the data acquisition system were then post-processed with the Aeroprobe software Aeroflow 2, in order to produce the velocity signals in physical units. Then the velocity signals are transformed from the ULM fixed reference frame to the Earth reference frame. The next step consisted in subtracting the velocities measured by the GPS during the flight in order to evaluate the wind velocity. For the post process the instantaneous temperature is also considered for temperature correction. Rejection and filtering of the data was performed by means of the inertial forces measured through the GPS/IMU unit. Indeed, in case of intense manoeuvring or strong gust, the wind velocity values were rejected.

6.2.4. LiDAR measurements

3D wind turbulence measurements were performed through three synchronous scanning Doppler wind LiDARs. The LiDARs used were StreamLine built by Halo Photonics. The 3D measurement technique was carried out by following the procedure described in Fuertes et al. (2014). Single point measurements were performed at heights of 50, 100, 150 and 200 m, while the exact location of the measurement points was evaluated precisely through a GPS system.

The LiDAR measurements are aimed at the assessment of the ULM turbulence measurements. Indeed, the ULM crossed the different measurement points selected by the LiDARs. In this way LiDAR measurements and ULM data are simultaneously available. Typical vertical profiles of the horizontal velocity of the wind are reported in Figure 25. The peculiar wind veer and shear is clearly detected with the LiDAR measurements.

6.2.5. Discussion and conclusions

Four days of ULM turbulence measurements were performed during the second field campaign on 8th, 21st, 28th and 30th May 2014. A very compact and robust setup is now achieved. No failure or drawbacks of the experimental setup were experienced during the last campaign. Indeed, 100% of the available time was used for measurements performance. The first setup required slightly more than 2 hours, including installation of the boom, setup of the probes, power supply and run on and monitoring of the acquisition system. The following setups required only 30 minutes.

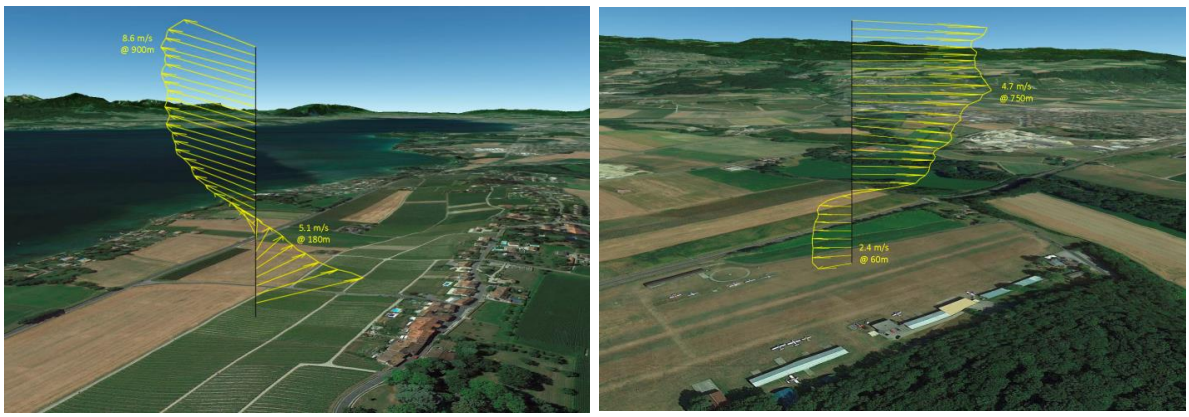

(a) (b)

Figure 25: vertical profiles of the horizontal velocity component of the wind obtained through three synchronous wind LiDARs: a) measurements performed in proximity of the shore in Rolle; b) measurements performed over the runway of the Prangins airport.

The main limitation for this campaign was represented by the rough atmospheric conditions. Indeed, besides rainy conditions, also days with wind velocity larger than 10 knots were considered dangerous. Unfortunately, days with significant winds would be the most interesting. This critical point makes the ULM platform practically not suitable for atmospheric measurements. Furthermore, the stability of the ULM is very weak, thus any gust on the ULM produces significant fluctuations in the measurements that are difficult to retrieve during the data post-processing.

6.3. Field-scale measurements of a canopy wake near Lake Leman using multiple LiDARs

6.3.1. Project overview

Canopy wakes have been shown, in controlled wind tunnel experiments, to significantly affect the fluxes of momentum, heat and other scalars at the land and water surface over distances greater than 1 km (Markfort et al., 2014). Figure 26 shows a schematic of the structure of the atmospheric boundary layer as it transitions from a forest canopy to a lake. Unfortunately, there are currently no measurements of the velocity field downwind of a full-scale forest canopy to corroborate the wind tunnel findings. Point-based anemometer measurements of wake turbulence provide limited insight into the extent and details of the wake structure, whereas scanning Doppler wind LiDARs can provide information on how the wake evolves in space and varies over time.

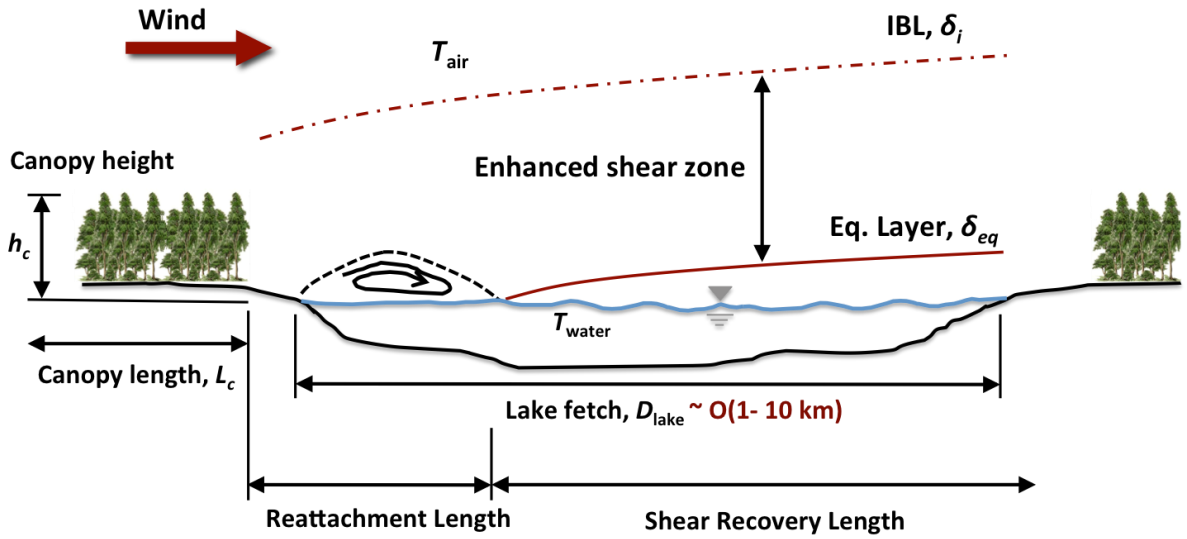

Figure 26. Schematic of wake zone and boundary layer growth at a tree canopy to lake transition (Markfort et al., 2014)

6.3.2. LiDAR Measurements

Using multiple scanning Doppler wind LiDARs, the team from WiRE Lab measured the velocity field in the wake of a tall tree canopy patch at Lake Leman. The patch consists of two uniform rows of 35-meter tall deciduous, plane trees, which border either side of the Allée de Dorigny, near the EPFL campus. The canopy is approximately 250 m long, and it is 35 m wide, along the direction of the wind. A challenge faced while making field measurements is that the wind rarely intersects a canopy normal to the edge. The resulting wake flow may be deflected relative to the mean inflow. Using multiple LiDARs, we measure the evolution of the wake due to an oblique wind blowing over the canopy (Figure 27). One LiDAR is positioned directly downwind of the canopy to measure the flow along the mean wind direction and the other is positioned near the canopy to evaluate the transversal component of the wind and how it varies with downwind distance from the canopy. Both are programmed to perform Range Height Indicator (RHI) scans to measure the velocity distribution and veer downwind of the canopy. A third LiDAR is employed in a staring mode to measure the time-varying velocity from near the top of the canopy and within the wake.

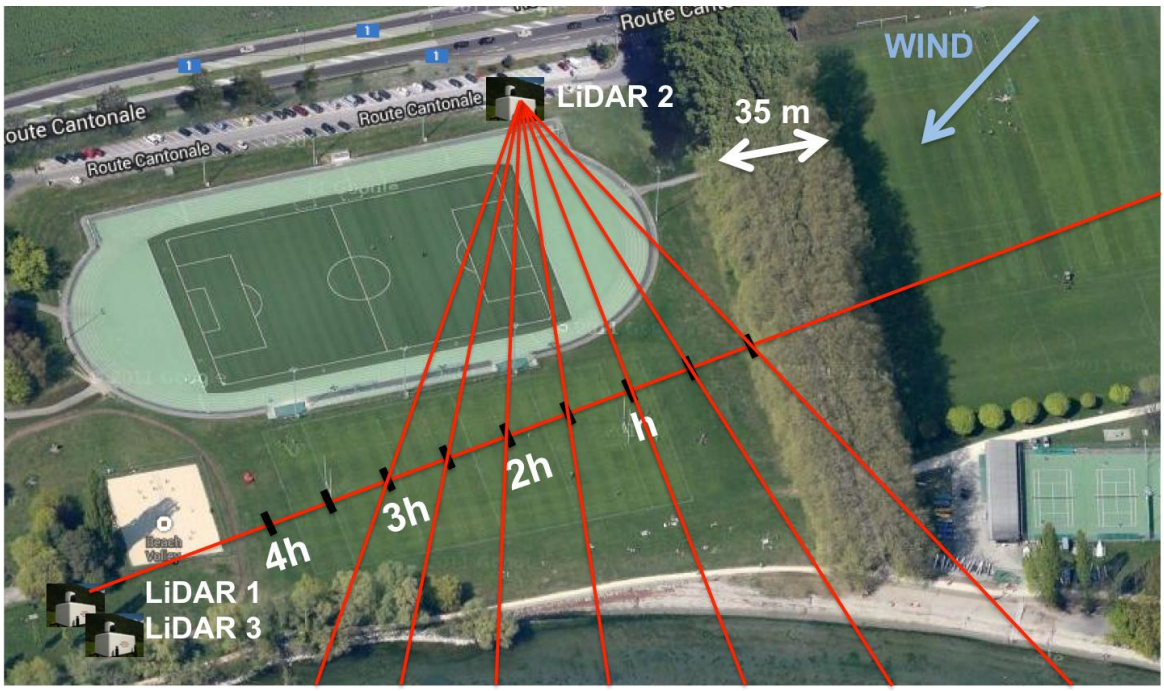

Figure 27. Set up for the canopy-patch wake experiment. LiDAR 1 measures turbulence over and in the wake of the canopy patch, while LiDAR 2 and 3 measure the mean velocity field.

6.3.3. Preliminary results

Based on the initial analysis of the data from the scanning Doppler wind LiDARs, we are able to detect the evolution and variability of the wind field in the wake of a canopy patch. In particular we have found the following:

- Using multiple LiDARs, we are able to characterize, for the first time, the evolution of the wake due to an oblique wind blowing over the canopy (Figure 28).
- Open trunk space near the base of the canopy results in a surface jet that can be detected just downwind of the canopy and further downwind dissipates as it mixes with the lower momentum wake flow above (Figure 29)
- We observed higher turbulence at canopy height in the wake compared to at the ground

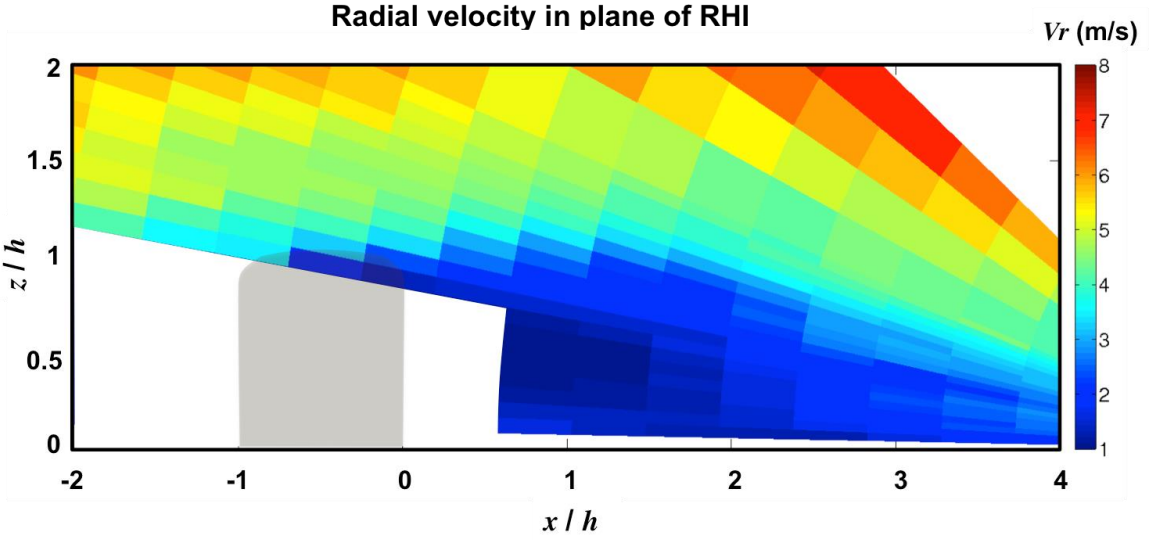

Figure 28. Ensemble average radial velocity from RHI scans collected for one hour under stationary and neutrally buoyant conditions. The canopy patch is indicated by a gray box bound between x/h: (-1,0), and z/h: (0,1).

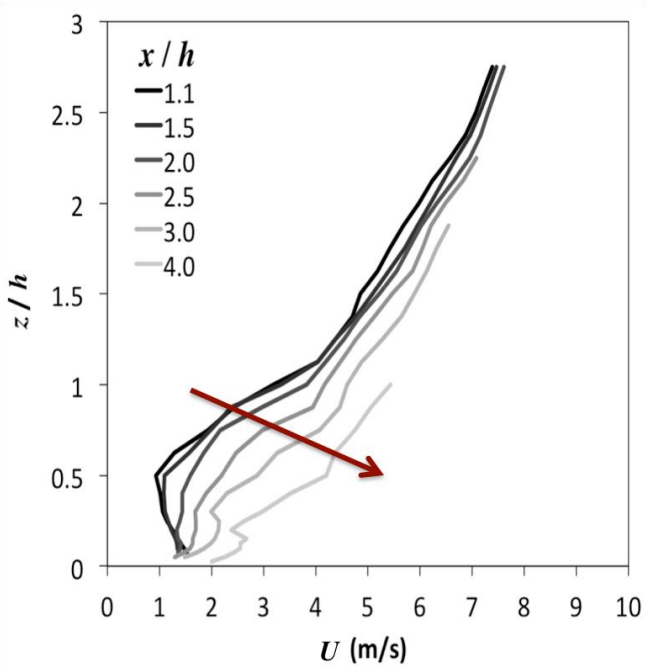

Figure 29. Profiles of mean horizontal velocity in the wake of the canopy patch, as measured by LiDAR. The red arrow indicates increasing downwind distance.

6.3.4. Preliminary discussion and outcomes

These results support previous laboratory findings indicating failure of the constant flux layer over complex and heterogeneous landscapes, where wake turbulence dominates. Further analysis is planned to assess the implications of canopy wakes for measurement and modelling of surface fluxes will be discussed. This work has been presented in April, 2014 at the EGU General Assembly in Vienna, Austria. An update of the analysis for different seasons with varying leave density will be presented at the AGU Fall Meeting in December, 2014 in San Francisco, California. A manuscript is in preparation that will provide new insights on the complex flow in the wake of forest canopies and how wakes within the atmospheric boundary layer impact surface fluxes at the air-water interface (Markfort et al., *In Preparation*).

7. Princeton effort in collaboration with EFLUM/CRYOS

Prof. M Hultmark, G. Arwatz, Dr. H Huwald and Prof. M B Parlange

7.1. Objective

The goal for the Princeton part of this effort is to develop new and unique ultra-fast-response temperature and humidity sensors. These sensors are designed to enable unprecedented investigations of the full range of turbulent scales present in the atmospheric boundary layer. In combination with velocity measurements an accurate estimate of the latent heat and sensible heat flux from the surface can be made. Additionally, the turbulent humidity, temperature spectrum and their co-spectrum can be calculated and compared to existing models.

7.2. Sensor development

Early in the development stage of the humidity sensor, it was observed that the state of the art temperature sensors were lacking in frequency response. This resulted in a need to first develop an accurate fast response temperature sensor.

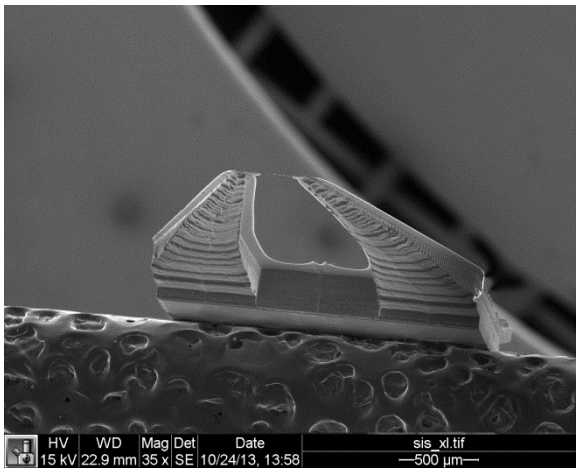

Figure 30: MEMS temperature sensor (T-NSTAP)

A model to describe the dynamics of cold-wires was developed (Arwatz et al., 2013). This model was used to design an improved temperature sensor. A MEMS-based temperature sensor have been successfully manufactured (T-NSTAP, see Figure 30) using techniques previously developed for a velocity sensors (NSTAP). The design of the T-NSTAP is such that it minimized end-conduction effects, and thus minimizes low frequency attenuation of the measured temperature signal. By making the wire very thin, the thermal mass can be kept low to improve the high frequency behaviour. A test bench was built consisting of an alternating hot and cold jet which allows us to study the frequency response of the T-NSTAP (see Figure 31). The results indicate that the new sensors are several orders of magnitude faster than conventional cold-wires. A detailed description of the T-NSTAP and the comparison to conventional cold-wires can be found in Arwatz *et al.* (MST, Under review).

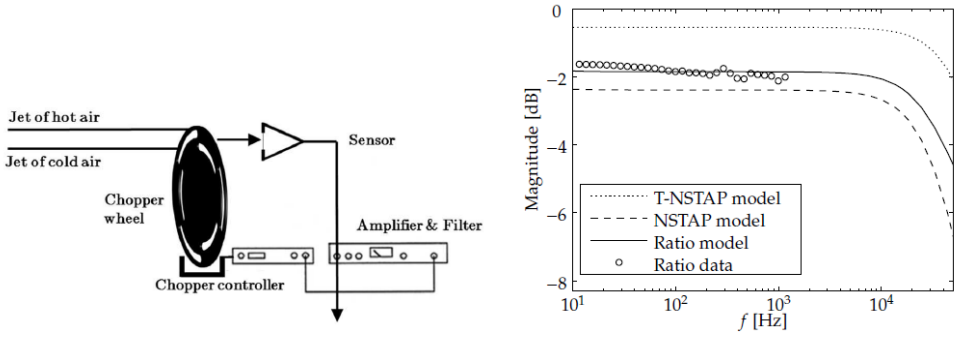

Figure 31: Schematic of test setup and resulting Bode plot

With a substantially improved temperature sensor, the work on the humidity sensor has resumed. In order to measure fast-response humidity we have been developing a brand new sensor based on a previously unexplored principle. For the humidity sensor a nano-wire is heated by Joule heating. The small characteristic length scale of the wire results in a Peclet number less than unity. A low Peclet number indicates that molecular diffusion of heat dominates over convection of heat away from the wire. This allows us to reduce the sensitivity to velocity and make a sensor that is mainly sensitive to thermal conductivity of

the surrounding fluid. The Peclet number is defined as $Pe = \frac{LU}{\alpha}$, (where L is the diameter of the wire, U the velocity over it and α the thermal diffusivity of the air). Since the thermal conductivity of the air is a strong function of water content, such a sensor will be able to detect changes in the water content.

In order to reduce the Peclet number, a sensor was manufactured consisting of a 10 μm long free-standing wire with 120 x 500 nm cross-section. The new sensor (q-NSTAP) is operated using a constant temperature feedback circuit. However, none of the commercially available systems were able to operate the new wire due to either over current or oscillations. Therefore, a custom-built circuit was developed with reduced current and increased adjustments of the feedback characteristics, to avoid oscillations. After many attempts a circuit was built that can successfully operate the q-NSTAP in a stable configuration. Due to the miniscule thermal mass of the wire, it can adapt to a change in the environment much faster than any sensor available. By exposing the sensor to a square wave in the current and observing the response its bandwidth can be approximated. The resulting response is shown in Figure 32, with a bandwidth close to 0.5 Mhz. This is almost 5 orders of magnitude faster than conventional humidity sensors. The q-NSTAP is ready to be tested in a humidity chamber, and can hopefully be tested in the field early next year.

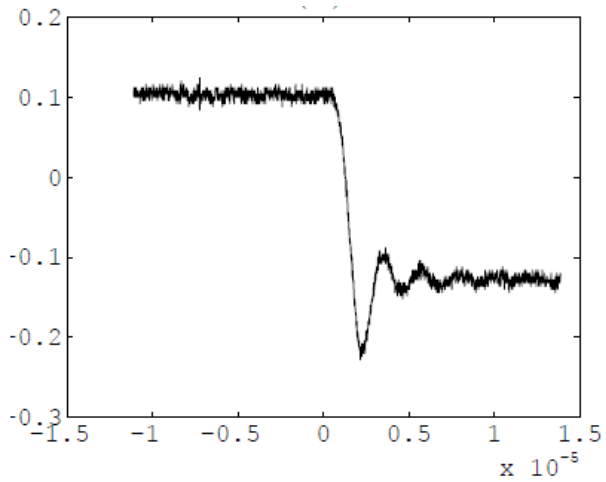

Figure 32: Square-wave test of the q-NSTAP sensor, indicating close to 0.5 MHz frequency response.

7.3. Field experiments

An experimental investigation to assess the feasibility of using nano-scale temperature sensors on the ULMs was carried out in a series of tests above Lake Leman. The new sensor had shown superior performance when compared to traditional cold wires in laboratory setting. However, the ultimate goal of the current study is to measure with the sensors over Lake Leman, mounted to the ULM. The combination of these measurements with velocity and position measurements by other groups guarantees unfiltered atmospheric data. To test the reliability in the field 6 nano-scale probes were installed on each side of a ULM's fuselage (as shown in Figure 33).

Figure 33: T-NSTAPs mounted on the side of the ULM fuselage.

Temperature data was acquired using specially designed constant current circuit (designed and built at Princeton University). The circuit is designed for low noise level and low sensitivity to ambient conditions. The autonomous data acquisition was installed on the ULM to acquire data during flight (as seen in Figure 34).

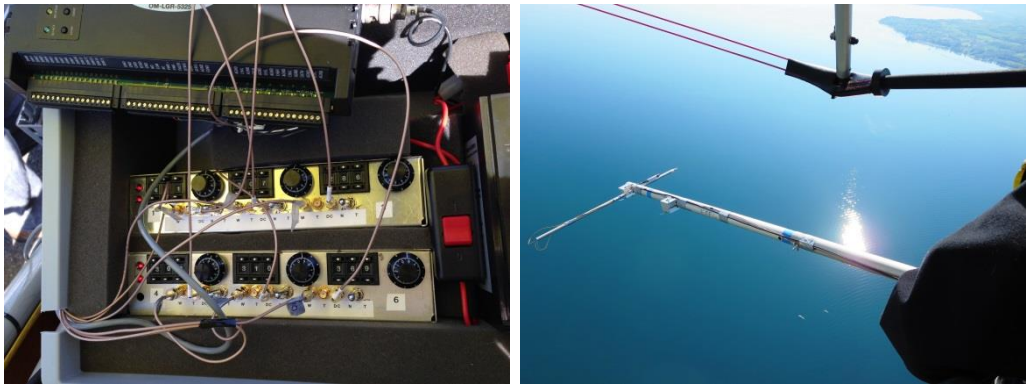

Figure 34 (a) On-board integration of the data acquisition and (b) the sensors during flight.

It was shown that the sensor performed well during various flight conditions. The sensors survived takeoff, landing and cruising at velocities up to 25 m/s. Due to lack of telemetry (GPS altitude and velocity) on the ULM at the time of tests, temperature data is of limited use. However, the feasibility and robustness of the sensors were tested and validated with great success.

8. Reference

Arwatz G, Bahri C, Smits A J and Hultmark M. (2013): Dynamic calibration and modeling of a cold wire for temperature measurement. Measurement Science and Technology (24): 125301. doi:10.1088/0957-0233/24/12/125301

Arwatz G, Fan Y, Bahri C and Hultmark M. (Under review): Development and characterization of a nano-scale temperature probe (T-NSTAP) for turbulent temperature measurement, Measurement Science and Technology.

Carbajo Fuertes F, Iungo GV, Porté-Agel F. (2014): 3D Turbulence Measurements Using Three Synchronous Wind Lidars: Validation against Sonic Anemometry, in Journal Of Atmospheric And Oceanic Technology, 31(7):1549-1556.

Doerffer R., and Schiller H. (2007): The MERIS Case 2 water algorithm. Int. J. Remote Sens. 28, 517–535.

Markfort CD, Porté-Agel F, Stefan HG. (2014): Canopy-wake dynamics and wind sheltering effects on Earth surface fluxes. Environmental Fluid Mechanics. 14(3):663-697. doi:10.1007/s10652-013-9313-4.

Markfort CD, Carbajo Fuertes F, Iungo GV, Stefan HG, Porté-Agel F. (2014): Canopy wake measurements using multiple scanning wind LiDARs. Abstract EGU2014-9401 presented at General Assembly of the European Geosciences Union, Vienna, Austria.

Markfort CD, Carbajo Fuertes F, Iungo GV, Stefan HG, Porté-Agel F. (2014): Canopy wake measurements using multiple scanning wind LiDARs. Abstract A43B-3268 presented at 2014 Fall Meeting, AGU, San Francisco, California.

Markfort CD, Carbajo Fuertes F, Iungo GV, Stefan HG, Porté-Agel F. (in preparation): Field-scale canopy-patch wake measurements using multiple scanning wind LiDARs.

Odermatt D, Giardino C, and Heege T. (2010): Chlorophyll retrieval with MERIS Case-2-Regional in perialpine lakes. Remote Sens. Environ. *114*, 607–617.